1 **On the Relationship Between Cloud Water Composition and Cloud Droplet Number**
2 **Concentration**

4 Alexander B. MacDonald[1], Ali Hossein Mardi[1], Hossein Dadashazar[1], Mojtaba Azadi Aghdam[1],
5 Ewan Crosbie[2,3], Haflidi H. Jonsson[4], Richard C. Flagan[5], John H. Seinfeld[5], Armin
6 Sorooshian[1,6*]
7
8 [1]Department of Chemical and Environmental Engineering, University of Arizona, Tucson, AZ,
9 USA
10 [2]Science Systems and Applications, Inc., Hampton, VA, USA
11 [3]NASA Langley Research Center, Hampton, VA, USA
12 [4]Naval Postgraduate School, Monterey, CA, USA
13 [5]Department of Chemical Engineering, California Institute of Technology, Pasadena, CA, USA
14 [6]Department of Hydrology and Atmospheric Sciences, University of Arizona, Tucson, AZ, USA
15
16 [*]Corresponding author: armin@email.arizona.edu

Abstract

Aerosol-cloud interactions are the largest source of uncertainty in quantifying anthropogenic radiative forcing. The large uncertainty is, in part, due to the difficulty of predicting cloud microphysical parameters, such as the cloud droplet number concentration (N_d). Even though rigorous first-principle approaches exist to calculate N_d, the cloud and aerosol research community also relies on empirical approaches such as relating N_d to aerosol mass concentration. Here we analyze relationships between N_d and cloud water chemical composition, in addition to the effect of environmental factors on the degree of the relationships. Warm, marine, stratocumulus clouds off the California coast were sampled throughout four summer campaigns between 2011 and 2016. A total of 385 cloud water samples were collected and analyzed for 80 chemical species. Single- and multi-species log-log linear regressions were performed to predict N_d using chemical composition. Single-species regressions reveal that the species that best predicts N_d is total sulfate ($R^2_{adj} = 0.40$). Multi-species regressions reveal that adding more species does not necessarily produce a better model, as six or more species yield regressions that are statistically insignificant. A commonality among the multi-species regressions that produce the highest correlation with N_d was that most included sulfate (either total or non-sea salt), an ocean emissions tracer (such as sodium), and an organic tracer (such as oxalate). Binning the data according to turbulence, smoke influence, and in-cloud height allowed examination of the effect of these environmental factors on the composition-N_d correlation. Accounting for turbulence, quantified as the standard deviation of vertical wind speed, showed that the correlation between N_d with both total sulfate and sodium increased at higher turbulence conditions, consistent with turbulence promoting the mixing between ocean surface and cloud base. Considering the influence of smoke significantly improved the correlation with N_d for two biomass burning tracer species in the study region, specifically oxalate and iron. When binning by in-cloud height, non-sea salt sulfate and sodium correlated best with N_d at cloud top, whereas iron and oxalate correlate best with N_d at cloud base.

1. Introduction

To assess the degree to which humans have altered Earth's climate, it is necessary to quantify the effect that particles in the air (i.e., aerosols) have on clouds. Some fraction of aerosols (called cloud condensation nuclei, CCN) activate into cloud droplets, thus impacting the cloud droplet number concentration (N_d). For warm marine boundary layer (MBL) clouds at fixed liquid water, higher N_d values result in (i) higher cloud albedo (thus cooling the Earth and counteracting the greenhouse effect) (Twomey, 1977), (ii) delayed and/or reduced precipitation (Albrecht, 1989), and (iii) enhanced entrainment at cloud top (Ackerman et al., 2004). The complex interactions and feedback mechanisms between aerosols, meteorology, and clouds leads to aerosol-cloud interactions as the largest source of uncertainty in climate models (IPCC, 2013; Bellouin et al., 2020).

It is indispensable to know the value of N_d, but this is a difficult parameter to accurately simulate and retrieve (Fountoukis & Nenes, 2005). There is a need to improve N_d retrievals from satellite remote sensors, which provide broad spatial and temporal coverage in contrast to surface sites and airborne research flights. Currently, N_d retrievals are limited to inferred values based on values of cloud optical depth, cloud droplet effective radius, and temperature, along with assumptions such as vertical homogeneity of N_d and monotonic increases in liquid water content at a constant fraction of its adiabatic value (Grosvenor et al., 2018). Ultimately, measurements are needed to better inform climate models about the cloud droplet activation process and better constraining N_d values. Current general circulation models (GCMs) calculate N_d using the properties of aerosol particles in one of two ways (Ghan et al., 1997; Menon et al., 2002). First, there is a rigorous approach that is based on physical principles that predicts N_d based on aerosol properties and meteorological conditions (Abdul-Razzak & Ghan, 2000). Second, there is an empirical approach that parameterizes N_d using either the number concentration of aerosols, N_a [# cm^{-3}], the number concentration of CCN, N_{CCN} [# cm^{-3}], or the mass concentration of chemical species that comprise the aerosols (Ghan et al., 1997).

The rigorous approach predicts N_d by considering aerosol properties (e.g., size distribution and chemical composition), microphysical processes (e.g., the seeding of cloud droplets by particles, droplet growth, and droplet evaporation), and meteorological parameters (e.g., relative humidity and the vertical updraft velocity transporting aerosols to cloud base) (e.g., Chuang et al., 1992; Chuang & Penner, 1995; Nenes & Seinfeld, 2003; Partridge et al., 2012). This method is based on the physical principle that an aerosol particle needs to be a CCN in order to seed a cloud droplet; consequently, the input for this approach is N_a, from which to calculate N_{CCN}, and subsequently N_d. The requisite information for these calculations may not be readily available for GCMs. A limitation is that the spatial resolution of a GCM may be too coarse to capture the small-scale spatial variation of updraft velocity (Ghan et al., 2011; West et al., 2014).

The empirical parameterization approach of interest in the present study uses the mass concentration of one or several chemical species and correlates it/them directly to N_{CCN} or N_d. Aerosols containing the sulfate ion (SO$_4^{2-}$) have long been known to serve as effective CCN (Andreae & Rosenfeld, 2008; Charlson et al., 1992; Lance et al., 2009; Medina et al., 2007). Sulfate is both contained in sea salt and is a product of the oxidation of gaseous sulfur dioxide (SO$_2$) (Hegg et al., 1981; Quinn et al., 2017), so it is customary to isolate the anthropogenic contribution to total SO$_4^{2-}$ by considering its non-sea salt fraction (NSS-SO$_4^{2-}$). Therefore, most studies choose either total SO$_4^{2-}$ (denoted hereafter as Tot-SO$_4^{2-}$) or NSS-SO$_4^{2-}$ to predict N_{CCN} and N_d (e.g., Leaitch et al., 1992; Novakov et al., 1994; Saxena & Menon, 1999). Using the mass

concentration of SO_4^{2-} or any other chemical species to predict N_d: (i) circumvents the complex intermediate microphysical steps to go from an aerosol particle to a cloud droplet and implicitly accounts for such meteorological variables like updraft velocity, (ii) is based on actual measurements, and (iii) can be compared directly to the mass concentration of different species produced by aerosol transport models (e.g., Boucher & Lohmann, 1995; Chen & Penner, 2005). The limitations of using an empirical parameterization are: (i) assuming a mass size distribution of the aerosols, (ii) assuming that one or a few chemical species are responsible for all CCN, and (iii) uncertainty in generalizing field data from one region (or a few regions) under specific conditions to the entire globe for all conditions (Pringle et al., 2009). Despite these drawbacks, empirical correlations of N_d and the mass concentration of different species are valuable. For example, of the 20 studies addressing the cloud albedo effect considered in the IPCC Fourth Assessment Report (IPCC, 2007), half relied on empirical relationships to calculate N_d (Pringle et al., 2009).

Several studies have developed empirical correlations between N_{CCN} and the mass concentration of SO_4^{2-} (e.g., Adams & Seinfeld, 2003; Hegg et al., 1993; Matsumoto et al., 1997). However, the present objective is to focus on improving the prediction of N_d, not N_{CCN}, using the mass concentration of SO_4^{2-} in addition to other species. A log-log relation is often used to correlate the mass concentration of SO_4^{2-} to N_d with an equation of the form (e.g., Lowenthal et al., 2004):

$$log(N_d) = a_0 + a_1 \, log([SO_4^{2-}]) \tag{1}$$

where $[SO_4^{2-}]$ is the mass concentration in air [µg m^{-3}], and a_0 and a_1 are fitting parameters. A log-log relation is chosen to accommodate large ranges in N_d and SO_4^{2-} and to reduce sensitivity of results to the measurement accuracy of each individual parameter (Boucher & Lohmann, 1995). The mass concentration of SO_4^{2-} can be obtained by analyzing either aerosol particles or cloud water. When analyzing cloud water, the mass concentration of SO_4^{2-} dissolved in droplets [mg lit^{-1}] is converted to the air-equivalent mass concentration [µg m^{-3}] by multiplying by the liquid water content, LWC [g m^{-3}], in a cloud. The data used to create N_d-SO_4^{2-} empirical parameterizations are typically derived from field campaigns, which differ in the region of analysis, sampling platforms (aircraft or ground-based), measurement approach (e.g., in particle form or dissolved in cloud water), and number of species analyzed. While the literature evaluating relationships between cloud water composition and N_d is limited and largely from aircraft studies from more than a decade ago, there is a growing number of datasets characterizing N_d and cloud water composition that are of interest to continue this line of research. Examples include the recently completed Cloud, Aerosol, and Monsoon Processes Philippines Experiment (CAMP^{2}Ex) and the North Atlantic Aerosols and Marine Ecosystems Study (NAAMES) (Behrenfeld et al., 2019), and the current multi-year Aerosol Cloud meTeorology Interactions oVer the western ATlantic Experiment (ACTIVATE) (Sorooshian et al., 2020). A summary of relevant past field work follows.

Leaitch et al. (1986) sampled continental stratiform and cumuliform clouds over Ontario, Canada and showed a roughly linear relationship between N_d and SO_4^{2-} at low SO_4^{2-} concentrations (below ~ 5 µg m^{-3}), and that the relationship leveled out at higher concentration (Novakov et al., 1994). Leaitch et al. (1992) suggested that the low R^2 values for the linear regression between N_d and SO_4^{2-} for both continental stratiform and cumuliform clouds (0.30 and 0.49, respectively) stemmed from factors such as (i) other chemical species besides SO_4^{2-}, and

139 variability in both (ii) updraft wind speed and (iii) temperature. Pueschel et al. (1986) sampled
140 clouds originating from marine and continental air masses at a ground-based observatory at
141 Whiteface Mountain, New York. They found that emissions contributed strongly to SO_4^{2-}, and
142 that a significant portion of SO_4^{2-}-containing particles acted as CCN, and thus likely impacted
143 N_d. Novakov et al. (1994) sampled marine cumulus and stratocumulus clouds by El Yunque peak
144 in Puerto Rico. Although they showed that N_{CCN} and SO_4^{2-} were highly correlated in both
145 cumulus and stratocumulus clouds, they also found that N_d and SO_4^{2-} were weakly correlated for
146 stratocumulus clouds, and not correlated for cumulus clouds. They attributed this difference to
147 the effect of entrainment and mixing on cloud microphysics. Leaitch et al. (1996) sampled
148 marine stratus clouds over the Gulf of Maine and the Bay of Fundy during the North Atlantic
149 Regional Experiment (NARE) and showed that SO_4^{2-} was better correlated with N_d than nitrate
150 (NO_3^-) (with an R^2 of 0.30 and 0.12, respectively). The R^2 between N_d and SO_4^{2-} increased when
151 the data were stratified into bins of low and high turbulence, which was quantified as the
152 standard deviation of vertical wind speed. They found that in situations with lower
153 supersaturations, N_d was more influenced by turbulence than by either SO_4^{2-} or N_a. Menon &
154 Saxena (1998) and Saxena & Menon (1999) sampled orographic clouds at a ground-based station
155 at Mt. Mitchell, North Carolina. They found that SO_4^{2-} was the main contributor to cloud water
156 acidity and a reliable tracer for anthropogenic pollution. Log-log regressions of SO_4^{2-}-N_d were
157 binned according to the level of SO_4^{2-}, with not much difference observed between the different
158 levels of pollution. Borys et al. (1998) and Lowenthal & Borys (2000) sampled warm marine
159 stratiform clouds on the Island of Tenerife in the Canary Islands. They found that N_d was
160 influenced by NSS-SO_4^{2-}, NO_3^-, pollution-derived trace elements, and elemental carbon (EC),
161 signifying that species other than SO_4^{2-} influenced N_d. Despite the sampling site's proximity to
162 African deserts, the mass concentration of crustal elements contained in dust was found to have
163 little correlation with N_d. Also, the sea salt tracer sodium (Na^+) was found to have little
164 correlation with N_d. Several studies (e.g., Boucher & Lohmann, 1995; Lowenthal et al., 2004;
165 Menon et al., 2002; Van Dingenen et al., 1995) have combined field data, such as those
166 mentioned above, in addition to other data sets, with the intention of producing a robust
167 empirical prediction of N_d. Menon et al. (2002) provided a log-log multi-species prediction of N_d
168 using SO_4^{2-}, organic matter, and sea salt. Organic carbon has been shown to increase N_d, as it
169 affects the surface tension of cloud droplets (e.g., Facchini et al., 1999; Nenes et al., 2002).
170 Additionally, nitric acid (HNO_3) has been linked with increased CCN activity and N_d based on
171 modeling studies (Hegg, 2000; Kulmala et al., 1993; Xue & Feingold, 2004).
172   McCoy et al. (2017) used N_d data from the Moderate-Resolution Imaging
173 Spectroradiometer (MODIS) satellite instead of in situ measurements. Second, aerosol mass
174 concentration data were obtained from the Modern-Era Retrospective Analysis for Research and
175 Applications version 2 (MERRA-2; Gelaro et al., 2017) reanalysis product and various aerosol
176 transport models instead of in situ measurements. Third, the study region was more global in
177 nature (albeit focusing on marine stratocumulus clouds) instead of a specific region. Fourth,
178 since reanalysis data were used, a multi-species, multi-variable linear regression was performed:
179
180 $$log(N_d) = a_0 + a_1\,log(SO_4^{2-}) + a_2\,log(SS) + a_3\,log(BC) + a_4\,log(OC) + a_5\,log(DU) \quad (2)$$
181
182 where SS is sea salt, BC is black carbon, OC is organic carbon, and DU is dust. McCoy et al.
183 (2017) found that SO_4^{2-} was predominantly correlated with N_d, with sea salt, black carbon,
184 organic carbon, and dust accounting for smaller contributions. A caveat to consider when

comparing the findings of McCoy et al. (2018) to other aircraft studies is that McCoy et al. (2018) used mass concentrations retrieved exclusively at the 910 hPa model level (~ 915 m), and only considered mass concentrations pertaining to submicron SS/DU and hydrophilic BC/OC.

The field studies cited above still leave a series of unanswered questions that the current study aims to address: (i) How is the SO_4^{2-}-N_d relationship affected by vertical wind speed (Leaitch et al., 1992), turbulence (Leaitch et al., 1996), and entrainment (Novakov et al., 1994)?; (ii) Why do species such as sea salt and dust play such a minor role in influencing N_d, even when located over the ocean and near a desert (Borys et al., 1998; McCoy et al., 2017, 2018)?; (iii) What is the relationship between organic matter and N_d (McCoy et al., 2018; Nenes et al., 2002)?; and (iv) Can the SO_4^{2-}-N_d correlation be improved by considering other chemical species (e.g., Hegg et al., 1993; Leaitch et al., 1992; Novakov & Penner, 1993)?. The present study will examine these questions using a data set comprised of in situ aircraft measurements collected off the California coast during four field campaigns. In addition to meteorological and aerosol and cloud microphysical measurements, a total of 385 cloud water samples were collected and analyzed for 80 chemical species (ions and elements). Even though measurements were collected in only one localized region, it is expected that the variety of conditions encountered over four summers, together with the large number of chemical species analyzed, will help address the questions noted above. The results of this work have implications for simulations and retrievals of N_d, in addition to studies examining relationships between atmospheric chemistry and cloud microphysics.

2. Methodology
2.1. Aircraft campaigns and study region

This work reports results relevant to warm marine stratocumulus clouds off the California coast based on field measurements from four field campaigns between 2011 and 2016, each during the months of July and August. The persistent summertime stratocumulus cloud deck located off the California coast offers the ideal natural laboratory to study aerosol-cloud-precipitation-meteorology interactions (Russell et al., 2013; Sorooshian et al., 2018). For all field campaigns, the Center for Interdisciplinary Remotely-Piloted Aircraft Studies (CIRPAS) Twin Otter was deployed out of Marina, California with an almost identical instrumentation payload. The four campaigns addressed in this study are: the Eastern Pacific Emitted Aerosol Cloud Experiment (E-PEACE) (Russell et al., 2013; Wonaschütz et al., 2013), the Nucleation in California Experiment (NiCE) (Crosbie et al., 2016; Maudlin et al., 2015), the Biological and Oceanic Atmospheric Study (BOAS) (Wang et al., 2016), and the Fog and Stratocumulus Evolution (FASE) Experiment (Dadashazar et al., 2017; MacDonald et al., 2018). Research flight information and tracks are shown in Table 1 and Figure 1, respectively.

Previous studies have used back-trajectory analysis to show that air in the MBL in the study region is predominantly influenced by air mass transport from the north and northwest (Schlosser et al., 2020; Wang et al., 2016; Wonaschütz et al., 2013). Thus, the cloud water in this study was influenced by a variety of local and long-range sources such as ship exhaust (Chen et al., 2012; Coggon et al., 2012), biomass burning (Prabhakar et al., 2014; Mardi et al., 2018), ocean emissions (Dadashazar et al., 2017; MacDonald et al., 2018), continental pollution (Ma et al., 2019; Wang et al., 2016), and dust (Mardi et al., 2019; Wang et al., 2014).

2.2. Aircraft instrumentation

230   Aircraft instrumentation used in each campaign is described in detail in Sorooshian et al.
231   (2018). The relevant instrumentation used in the present study is as follows: aerosol size
232   distribution was measured using a Passive Cavity Aerosol Spectrometer Probe (PCASP; particle
233   diameter (D_p) ~ 0.1–2.6 μm; Strapp et al., 1992); cloud droplet size distribution was measured
234   using a Forward Scattering Spectrometer Probe (FSSP; D_p ~ 2–45 μm; Gerber et al., 1999) and a
235   Cloud and Aerosol Spectrometer-Forward Scattering (CASF; D_p ~ 1–61 μm; Baumgardner et al.,
236   2001); rain drop size distribution was measured using a Cloud Imaging Probe (CIP; D_p ~ 25–
237   1600 μm; Baumgardner et al., 2001); cloud liquid water content (LWC) was measured using a
238   Particulate Volume Monitor (PVM-100A; D_p ~ 3–50 μm; Gerber, 1994); three-dimensional wind
239   speeds were calculated by combining the pressure measurements from a five-hole radome gust
240   probe plumbed into the aircraft nose together with the aircraft velocity and altitude
241   measurements provided by the aircraft's Global Positioning System/Inertial Navigation System
242   (GPS/INS).
243   Since LWC played a critical role in converting aqueous concentration to air-equivalent
244   concentration, the size range used to calculate N_d was bracketed to resemble the size range of the
245   PVM-100A. Therefore, N_d was defined in this study to be equivalent to the integration of the
246   cloud droplet size distribution between D_p ~ 3–50 μm, and was calculated using CASF (for E-
247   PEACE) and FSSP (NiCE, BOAS, and FASE). For the NiCE campaingn, LWC measurements
248   from the PVM-100A instrument were unreliable; therefore, the LWC for NiCE was calculated
249   instead using FSSP data between D_p ~ 3–50 μm.

2.3. Cloud water collection and chemical analysis

252   A total of 385 cloud water samples were collected throughout the four campaigns using a
253   modified Mohnen slotted-rod collector, reported to collect droplets with D_p ~ 5–35 μm (Hegg
254   and Hobbs, 1986). The cloud water was collected in polyethylene bottles and stored at ~ 5°C for
255   subsequent offline chemical analysis. The spatially-averaged location of each cloud water sample
256   is shown in Figure 1. Cloud water samples were chemically analyzed post-flight for ions using
257   ion chromatography (IC; Dionex ICS-2100) and for elements using inductively coupled plasma
258   mass spectrometry (ICP-MS; Agilent 7700 Series) for E-PEACE, BOAS, and NiCE or triple
259   quadrupole inductively coupled plasma mass spectrometry (ICP-QQQ; Agilent 8800 Series) for
260   FASE. The limit of detection (LOD) for each ion and element measured is shown in Table S1.
261   The concentration of non-sea salt (NSS) species was calculated using the relative abundance of a
262   NSS species to Na^+ in natural sea salt (Seinfeld & Pandis, 2016). Cloud water sample acidity was
263   quantified by measuring pH (the aqueous concentration of hydrogen ions, H^+) using a Thermo
264   Scientific Orion 9110DJWP Combination Semi-Micro pH Electrode for E-PEACE, NiCE, and
265   BOAS, and a Thermo Scientific Orion 8103BNUWP Ross Ultra Semi-Micro pH probe for
266   FASE. Aqueous concentrations (i.e., mass concentrations in the droplets [mg L^{-1}]) were
267   converted to air-equivalent concentrations (i.e., mass concentrations in the air [μg m_{air}^{-3}]) by
268   multiplying aqueous concentrations by the LWC and dividing by the mass density of water. This
269   study uses air-equivalent concentrations for all species with the exception of H^+ (pH) that uses
270   aqueous concentration.
271   A total of 80 species (29 measured ionic species, 46 measured elemental species,
272   measured pH, and 4 NSS calculated species; Table 2) were considered in this study as an initial
273   pool of candidate species that could potentially be used to predict N_d. To facilitate the statistical
274   analysis in this study, the amount of chemical species were filtered from 80 to only nine. The
275   steps used in this filtering process are summarized in the next section.

276
2.4. Filtering of chemical species

A focus in this study is to identify appropriate chemical species to use as predictors in a linear regression model (addressed in Section 2.5). Good statistical practice (e.g., Freund et al., 2010) recommends that two conditions must be met to produce a meaningful multivariable regression: (1) the independent/predictor variables must not be redundant, i.e., they must not be highly correlated among themselves (the property of high correlation is called collinearity), and (2) each independent/predictor variable must have some correlation with the dependent/response variable. There is no universal rule to define what is "highly" correlated, rather, it depends on the nature of the data and the user's judgement.

As using all 80 species is impractical in terms of providing results that could be tested and/or used by others, a filtering method was used to reduce the number of species. The filtering method consisted of seven steps (Figure 2), the objective of which was to trim the total number of species by an order of magnitude, leaving just a few that exhibited the following characteristics: (1) the most data quality and quantity, (2) the least redundancy among themselves, (3) the highest correlation with N_d, and (4) the most physical meaning. The decision to remove a species becomes less objective and quantifiable towards the last steps in Figure 2. Each step is described below.

Step 1 removed species with less than 70% of data points. A species could have a low amount of points because it was not analyzed in a field campaign or because the data quality from the IC or ICP (ICP-MS or ICP-QQQ) was inadequate. Step 2 removed duplicate species that were measured by both IC and ICP. Step 3 addressed Condition (2) by removing species that were collinear (i.e., correlated among themselves). The criterion for a "high" correlation was to have a correlation coefficient (R) > 0.6 and a p-value < 0.05. For example, if a fixed number of five species were all highly correlated between each other, then only one of the five species was kept, and the rest were removed. This procedure is to consolidate "families" of three or more highly correlated species to a single species and does not apply to pairs of highly consolidated species. Step 4 addressed Condition (3) by removing species that were not correlated to N_d. The criterion for a "low" correlation was to have a coefficient of determination (R^2) < 0.1. Notice that Step 3 uses R whereas Step 4 uses R^2; this is because collinearity is determined not only by the value of R but also the sign of R. Step 5 removes all but one organic species, oxalate (Ox), since this species generally had the highest mass concentration of all the organic species and was considered to be representative of all other organic species. Step 6 removed species that could not easily be attributed to a physical process or chemical source. Step 7 added back into the analysis four species that had been removed. This was done for the sake of having species that are known to have relevant sources in the study region. Even though pH plays an important role in the partitioning of gases into particles and droplets, in addition to influencing aqueous reactions in droplets (e.g., Pye et al., 2020), pH was filtered out in Step 4 for being a poor predictor of N_d.

The nine species that survived the filtering scheme in Figure 2 are methanesulfonic acid (MSA), ammonium (NH_4^+), NO_3^-, Ox, Tot-SO_4^{2-}, NSS-SO_4^{2-}, Fe, Na, and vanadium (V). These species have known sources as follows. MSA: ocean biogenic (Sorooshian et al., 2009); NH_4^+: agriculture (Bauer et al., 2016), marine emissions (Bouwman et al., 1997), and wildfires (Reid et al., 1998); NO_3^- and Ox: fire (Prabhakar et al., 2014; Maudlin et al., 2015); Tot-SO_4^{2-}: sea salt (Seinfeld & Pandis, 2016), ocean biogenic (Charlson et al., 1987), and shipping (Coggon et al., 2012), with NSS-SO_4^{2-} missing the sea salt contribution; Fe: dust (Jickells et al., 2005) and fire

322 (Maudlin et al., 2015); Na: sea salt (Seinfeld & Pandis, 2016); V: shipping (Wang et al., 2014).
323 Note that we retained both Tot-SO_4^{2-} and NSS-SO_4^{2-}; this is to evaluate which correlates more
324 with N_d, as some studies have used Tot-SO_4^{2-} (e.g., Leaitch et al., 1992; Saxena & Menon, 1999),
325 whereas other have used NSS-SO_4^{2-} (Novakov et al., 1994; Boucher & Lohmann, 1995).
326 Sections 3.1 and 3.2 will discuss these nine species, and the rest of Section 3 will focus on only
327 four species to be explained later. These species were analyzed by a multivariable regression
328 model, which is described in the next section.
329
330 **2.5. Mathematical model**
331   This study examines the relationship between cloud water mass concentration and N_d
332 with a multivariable linear model similar to that of McCoy et al. (2017, 2018):
333
334 $$log(N_d) = a_0 + a_1 \, log(M_1) + a_2 \, log(M_2) + \cdots + a_n \, log(M_n) \tag{3}$$
335
336 where M_i is the air-equivalent mass concentration of species i [µg m^{-3}], a_i are fitting parameters,
337 and n is the number of species being considered. N_d is the dependent (or response) variable, and
338 $M_1, M_2, \ldots, M_n$ are the independent (or predictor) variables. The logarithmic forms of N_d and M_i
339 were correlated to account for a numerically large range of several orders of magnitude, and
340 because a log-log model is commonly used to correlate chemical composition to N_d (e.g.,
341 Boucher & Lohmann, 1995; Menon et al., 2002; McCoy et al., 2017).
342   The Matlab software package was used to obtain multivariable linear regressions of the
343 form of Equation 3 using the method of ordinary least squares. The performance of a regression
344 was quantified using the coefficient of determination (R^2). However, when comparing the
345 performance of correlations between regressions using a different number of predictor variables,
346 it is necessary to use the adjusted coefficient of determination (R^2_{adj}), which is subscripted to
347 distinguish it from the ordinary R^2, and is adjusted by using the number of predictors (P) and the
348 number of data points (N) via the formula $R^2_{adj} = 1 - (1 - R^2)(N - 1)/(N - P - 1)$ (Kahane,
349 2008). For a large number of data points, $R^2_{adj} \sim R^2$; however, for the sake of rigor and
350 consistency, R^2_{adj} is used instead of the ordinary R^2, except when reporting values from the
351 literature. The statistical significance of correlations was quantified using the p-value obtained
352 by doing a two-tailed Student's t-test. Both R_{adj}^2 and p-values were given by the Matlab software
353 after regression. P-values were obtained for both the overall regression and each individual
354 coefficient in the regression, e.g., if a regression has three predictors, there are a total of five p-
355 values: one for the overall regression, three for the slope of each individual predicting variable,
356 and one for the intercept. In this study, a regression was considered to be statistically significant
357 if all the p-values were < 0.05.
358   The correct functioning of the method of ordinary least squares requires that the set of n
359 predicting variables in Equation 3 not be collinear. Multicollinearity is defined by a set of three
360 or more predicting variables being collinear. Using a set of multicollinear predictors can produce
361 unreliable estimates in both magnitude and sign of the coefficients (a_i) (Kahane, 2008). There is
362 no universal marker for multicollinearity. Furthermore, multicollinearity can only be addressed
363 when analyzing all predictors together. For example, for a given set of three predictors (P_1, P_2,
364 and P_3), even though the pairs P_1-P_2, P_1-P_3, and P_2-P_3 are not collinear, there is no guarantee that
365 the P_1-P_2-P_3 set is not multicollinear. When considering a complex system such as the chemical
366 composition of cloud water, it is reasonable to assume that as more species are used to predict

367 N_d, the higher the probability that the set of species is multicollinear. We did not test for
368 multicollinearity in this study; the consequences of not doing so are explored in Section 3.2.
369
370 **2.6. Calculation of turbulence**
371   Similar to Leaitch et al. (1992) and Feingold et al. (1999), this study analyzes the effect
372 of turbulence on the ability to predict N_d. Turbulence was considered to be represented by the
373 standard deviation of the vertical wind speed (w) and is represented as σ_w. Also similar to Leaitch
374 et al. (1992), this study classified conditions into turbulent and smooth regimes by considering
375 the upper and lower 33rd percentile of σ_w, respectively. Although the rigorous approach to
376 calculate σ_w uses the w from below the cloud (Twomey, 1959), this study used vertical wind
377 speed data collected throughout the sampling time (i.e., mostly inside the cloud, but also outside
378 the cloud). This was mainly because not all cloud water samples had an accompanying
379 measurement of w below the cloud. To justify using σ_w from the sampling time instead of below
380 cloud σ_w, consider Figure S1, which shows a representative time series of altitude, w, and σ_w for
381 a cloud water sample that was collected minutes before a below-cloud leg, which collected
382 measurements of w. It can be seen that the plots of w and σ_w are similar, and that an average σ_w
383 calculated either way is still in the bottom 33rd percentile. Therefore, for purposes of this study,
384 we consider in-cloud turbulence to reasonably approximate below-cloud turbulence.
385
386 **2.7. Determination of smoke influence**
387   One of the objectives of this study is to analyze the extent to which the presence of
388 smoke from wildfires affects the correlation between N_d and cloud water chemical composition.
389 Thus, it was important to identify cloud water samples that were influenced by smoke. Only the
390 NiCE and FASE campaigns were affected by wildfires. Mardi et al. (2018) identified vertical
391 soundings in the NiCE and FASE campaigns that were influenced by smoke by establishing
392 smoke influence to have a total aerosol number concentration (N_a) ≥ 1000 cm^{-3}, as measured by
393 the PCASP, in addition to visual and olfactory detection of smoke by flight scientists. In this
394 study, a cloud water sample was considered to be influenced by smoke if it was collected during
395 a research flight (RF) that contains a vertical sounding identified by Mardi et al. (2018) to be
396 influenced by smoke, even if the cloud water sample was not necessarily collected near the
397 sounding labelled as smoke-influenced; this is a valid assumption based on the work of Mardi et
398 al. (2019). The RFs considered to be smoke-influenced in this study were NiCE RFs 16–23 and
399 FASE RFs 3–11 and 13–15.
400
401 **3. Results and Discussion**
402   With the refined list of nine physically-meaningful species from Section 2.4, we now
403 proceed to address the following questions: (1) What single species best predicts N_d?; (2) How
404 many species are sufficient to predict N_d?; (3) What is an effective combination of species to
405 predict N_d?; and (4) How do several factors (i.e., turbulence, smoke-influence, and location along
406 cloud depth) affect the ability to reliably predict N_d? These questions are addressed in order in
407 Sections 3.1–3.4.
408
409 **3.1. Single-variable prediction of N_d**
410   In this section, we analyze which of the nine species filtered out in Section 2.4 best
411 predicts N_d by itself without binning by external factors. These single-predictor regressions with
412 no binning are important, as they provide a baseline for subsequent sections in which multi-

predictor regressions and binning are used. Table 3 and Figure 3 display the ability of each of the nine species to predict N_d. To have consistency with subsequent sections, R^2_{adj} is used instead of the ordinary R^2. The regression and the individual coefficients all were statistically significant.

Some previous studies predicted N_d using Tot-SO_4^{2-} (e.g., Leaitch et al., 1992; Saxena & Menon, 1999), whereas other studies used NSS-SO_4^{2-} (e.g., Novakov et al. 1994; Lowenthal et al., 2004). We find that Tot-SO_4^{2-} is the best predictor, and that is better correlated to N_d (R^2_{adj} = 0.40) than NSS-SO_4^{2-} (R^2_{adj} = 0.29). This is likely because Tot-SO_4^{2-} encompasses both sea salt particles and non-sea salt particles, and thus gives a better approximation to the total number concentration of CCN. In addition, Tot-SO_4^{2-} also had the largest slope (a_1 = 0.32), suggesting that N_d is more sensitive to changes in Tot-SO_4^{2-} than other chemical species. Although HNO_3 has been observed to increase N_d (e.g., Xue & Feingold, 2004), NO_3^- was found to be only moderately correlated with N_d (R^2_{adj} = 0.24). The species with the lowest correlation was Fe (R^2_{adj} = 0.05). This low correlation with N_d was also presented by other crustal metals like Al (R^2_{adj} = 0.01) and Ti ($R^2_{adj} \sim 0$) (not shown in Table 3). The low influence of crustal metals on N_d is consistent with the findings of Lowenthal & Borys (2000). Some physical meaning can be extracted from the intercept of the regression (a_0). If N_d is insensitive to the mass concentration of a species, then the slope (a_1) should be zero; and N_d would be constant with a value of $N_d = 10^{a_0}$. These intercepts yield a range of N_d of 108–412 cm^{-3}. These values are not unrealistic in clouds in this study region (e.g., Chen et al., 2012; Lu et al., 2009; Wang et al., 2016).

To contrast with results of this work, Table 4 shows the regression parameters from other studies when correlating N_d and SO_4^{2-}. For the sake of completeness, Table 4 shows regressions that analyzed non-marine stratocumulus clouds, but in this comparison, we focus only on those regressions that analyzed stratocumulus clouds. Our results (i.e., a_i coefficients and R^2) for Tot-SO_4^{2-} reasonably match the results of Leaitch et al. (1992), suggestive of commonality between two coastal regions with differing meteorological conditions (i.e., northeast Pacific vs northwest Atlantic) (Sorooshian et al., 2019). Our results for NSS-SO_4^{2-} also reasonably match those of McCoy et al. (2017), which is noteworthy as McCoy et al. (2017) used satellite retrievals and model aerosol concentrations for several stratocumulus decks around the world, whereas our analysis used in situ data from a relatively small region. However, our NSS-SO_4^{2-} results differ significantly from those of Novakov et al. (1994), which is understandable since the regression presented by Novakov et al. (1994) has a p-value > 0.05. Our data set does not achieve the degree of correlation achieved by Lowenthal et al. (2004), who report the highest correlation for marine clouds (R^2 = 0.82). The studies that analyzed stratocumulus clouds all report intercept values (a_0) ~ 2.0, which is consistent with our data.

3.2. Multi-variable prediction of N_d

When previous studies correlated N_d (or N_{CCN}) and the air-equivalent concentration of chemical species and obtained a poor correlation, it was suggested that taking more chemical species into consideration would improve the correlation (e.g., Leaitch et al., 1992; Novakov et al., 1994). In this this section we address the issue: "How many chemical species are necessary to adequately predict N_d?". To answer this question, we use the nine filtered species from Section 2.4. Regressions of the form of Equation 3 are performed for every combination of species. The number of predictors in the regressions are varied from one up to eight. The number of combinations (C) that can be made with P predictors selected from S species is $C = S!/(S-P)!$. Combinations that include Tot-SO_4^{2-} and NSS-SO_4^{2-} together are not considered, thus leaving a total of 383 regressions.

459   Of the total 383 regression, only 67 were considered as statistically significant. Figure 4
460 shows the R^2_{adj} as a function of the number of predictors for both statistically significant and
461 insignificant regressions; the percentage of regressions that were statistically significant is shown
462 in Table S2. These results show that adding more predictors does not necessarily improve the
463 correlation, as all correlations that use six or more predictors are statistically insignificant. This
464 behavior is perhaps because the new species being added are redundant with respect to the
465 species that are already in the model (i.e., the new species is mathematically collinear with the
466 old species). It is also interesting to note how R^2_{adj} increases asymptotically to ~ 0.6; this further
467 makes the point that additional species do not necessarily improve predictability of N_d. The same
468 asymptotic behavior is also exhibited with R^2, as R^2 and R^2_{adj} for these regressions differ by only
469 ~ 2%.
470   We examined the best regressions produced by a given number of predictors to explore
471 the factors that contribute to a respectable multivariable regression. Table 5 shows the three
472 statistically significant regressions that had the highest R^2_{adj} for a given number of predictors
473 (one to five). The predictors are ordered horizontally according to the value of their coefficient in
474 order to show qualitatively which species is more dominant in a regression. Eight of the nine
475 chemical species considered appear at least once in a regression, with the most common species
476 being NH_4^+, a form of SO_4^{2-} (total or non-sea salt), Na, Ox, and MSA. Sulfate (total or non-sea
477 salt) appears in 12 of the 15 regressions, and in eight regressions it has the largest coefficient;
478 this speaks to the importance of SO_4^{2-} in predicting N_d. However, the appearance of Na and Ox
479 and their non-negligible slope also highlights the importance of considering them as well in a
480 correlation; this is clearly observed in the increase of R^2_{adj} when Na and Ox are added to a
481 regression that contains only $NSS\text{-}SO_4^{2-}$ (Table 6). We believe that the ingredients that yield the
482 higher R^2_{adj} in Table 5 are: (1) a form of SO_4^{2-} (such $Tot\text{-}SO_4^{2-}$ or $NSS\text{-}SO_4^{2-}$), (2) a sea
483 emissions tracer (such as Na), and (3) an organic tracer (such as Ox). NH_4^+ was present in all the
484 regressions; however, given that it comes from diverse sources such as agriculture (ApSimon et
485 al., 1987; Bauer et al., 2016), marine emissions (Bouwman et al., 1997; Paulot et al., 2015), and
486 wildfires (Maudlin et al., 2015; Reid et al., 1998), it is difficult to assess if it contributes to the
487 CCN budget or simply accompanies all types of CCN. In other words, we suspect that NH_4^+
488 appears in all correlations because it generally accompanies the three ingredients we propose
489 make a good correlation: a form of SO_4^{2-}, a marine emissions tracer, and an organic tracer.
490   It is of interest to note that combining a sea salt tracer (such as Na) with $NSS\text{-}SO_4^{2-}$ in a
491 two-predictor model has about the same performance ($R^2_{adj} = 0.41$; Table 6) as a one-predictor
492 model using $Tot\text{-}SO_4^{2-}$ ($R^2_{adj} = 0.40$; Table 3). We believe this is because $Tot\text{-}SO_4^{2-}$ encompasses
493 the sea salt and the non-sea salt contribution to CCN about the same as the artificial
494 mathematical separation of the two. Also of interest is that when only looking at the statistically
495 significant regressions, only 17 regressions have species with negative coefficients (i.e., negative
496 slopes). The species with negative coefficients are NO_3^-, Fe, and V (not shown); more
497 specifically, NO_3^-, Fe, and V have negative coefficients when they are accompanied by NH_4^+ in
498 the same regression. The physical reason as to why these species have negative coefficients
499 when mixed with NH_4^+ is not clear; perhaps the reason is due to the mathematics of the
500 regression and not physically rooted, as multicollinearity can lead to unexpected magnitudes and
501 signs for predictor coefficients (Kahane, 2008). In addition, multicollinearity will become more
502 likely as more predictors as considered. Therefore, it is not surprising that unexpected negative
503 coefficients only appear when considering many (five) predictors. Lastly, a correlation matrix
504 among the nine predicting species (Figure S2) shows a strong correlation for some pairs of

505   species (NH_4^+-NO_3^-: R^2_{adj} = 0.48; NO_3^--V: R^2_{adj} = 0.49) and moderate correlation for other pairs
506   (NH_4^+-V: R^2_{adj} = 0.27; NO_3^--Fe: R^2_{adj} = 0.22), thus strengthening the argument that the negative
507   coefficients are due to mathematical multicollinearity and not a physical or chemical reason.

508   When considering a multi-species model to predict N_d, it is worthwhile to examine the
509   coefficient of sea salt. Even though it is well established that more CCN leads to more droplets,
510   the effect of giant CCN (GCCN), such as sea salt, is not as clear. Cloud microphysics studies
511   suggest two mechanisms by which more sea salt leads to less N_d: (1) The large size and highly
512   hygroscopic nature of sea salt causes these particles to activate into droplets before other smaller
513   particles. This reduces the amount of available water vapor and creates unfavorable conditions
514   for smaller particles to nucleate into droplets (e.g., Andreae & Rosenfeld, 2008). (2) GCCN
515   nucleate into larger droplets as compared to CCN, which in turn are more likely to collide and
516   coalesce with surrounding droplets. This combination of droplets creates larger but fewer
517   droplets and ultimately leads to the formation of rain drops and precipitation (e.g., Feingold et
518   al., 1999, Jung et al., 2015). Therefore, it is expected that the negative correlation between
519   GCCN and N_d should translate into a negative coefficient for Na (the sea salt tracer) in a multi-
520   predictor regression equation. However, this behavior was not observed in this study. A plausible
521   explanation for this discrepancy is that the effect of GCCN on N_d is highly dependent on
522   conditions like LWC and N_d itself (e.g., Feingold et al., 1999), and that this study did not capture
523   the appropriate conditions to observe this effect. However, McCoy et al. (2017) did observe a
524   negative coefficient for sea salt and ascribed it to a simulation artefact caused by the intimate
525   link between sea salt generation and wind speed (i.e., turbulence). An attempt to isolate the
526   effects of sea salt and turbulence on N_d is provided in Section 3.1.1.

527   Menon et al. (2002) and McCoy et al. (2017, 2018) are among the few studies that have
528   used multiple species to predict N_d (Table 7). Menon et al. (2002) used three species (sulfate,
529   organic matter, and sea salt). McCoy et al. (2017, 2018) used five species (sulfate, sea salt, black
530   carbon, organic carbon, and dust), but the 2017 study found the contribution of organic matter to
531   be negligible. In order to intercompare results with previous studies, we selected species
532   homologous to those of McCoy et al. (2017, 2018). We select NSS-SO_4^{2-} for sulfate, Na for sea
533   salt, oxalate for organic carbon, and Fe for dust. We did not measure a species analogous to
534   black carbon. The subsequent analysis examines only these four species using single-predictor
535   regressions.

536

537   **3.3. Analysis of meteorological factors through binning**
538   Historically, the effect that meteorological factors have on the composition-N_d (or -N_{CCN})
539   empirical relationship has been examined by analyzing regressions after binning by turbulence
540   (Leaitch et al., 1996), cloud type (Leaitch et al., 1992; Novakov & Penner, 1993), and region
541   (McCoy et al., 2018). The following sections address the effects of turbulence, smoke influence,
542   and location along cloud depth.

543

544   **3.3.1. Effect of turbulence**
545   Building upon the work of Leaitch et al. (1996), who studied how turbulence affects the
546   correlation between Tot-SO_4^{2-} and N_d, this study extends that analysis to examine four additional
547   species. Similar to Leaitch et al. (1996), this study quantified turbulence by the standard
548   deviation of vertical wind speed (σ_w). Our range of σ_w was 0.10–0.51 m s^{-1}. Low turbulence was
549   considered to be in the bottom 33rd percentile ($\leq$ 0.27 m s^{-1}), whereas high turbulence was taken
550   to be values in the top 33rd percentile ($\geq$ 0.33 m s^{-1}). Leaitch el al. (1996) considered low and

551 high turbulence to be $\sigma_w < 0.17$ m s^{-1} and $\sigma_w > 0.23$ m s^{-1}, respectively, and it is worth noting that
552 only five of our 385 samples are considered low turbulence according to the criterion of Leaitch
553 et al. (1996). Figure 5 and Table 8 show how R^2_{adj} depends on the predicting species and the
554 turbulence regime; the scatterplots from which the R^2_{adj} are taken are shown in Figure S3.

555   For NSS-SO$_4^{2-}$, there is no significant difference in R^2_{adj} when comparing all the points or
556 by binning by σ_w. However, this is not the case for Tot-SO$_4^{2-}$, in which there is a large difference
557 in the degree of correlation ($R^2_{adj} = 0.27$ and $R^2_{adj} = 0.55$ for low σ_w and high σ_w, respectively).
558 This is in agreement with Leaitch et al. (1996), in which the correlation (albeit, not log-log)
559 between Tot-SO$_4^{2-}$ and N_d yielded an $R^2 = 0.53$ and $R^2 = 0.91$ for low and high σ_w, respectively.
560 The difference in the behavior between Tot-SO$_4^{2-}$ and NSS-SO$_4^{2-}$ hints that the sea salt
561 contributions to SO$_4^{2-}$ (i.e., ocean-derived species) are the ones affected by turbulence, and hence
562 explains the insensitivity NSS-SO$_4^{2-}$ has to turbulence.

563   For Ox, the correlation improves at low turbulence ($R^2_{adj} = 0.30$), but not at high
564 turbulence ($R^2_{adj} = 0.09$). We believe Ox behaves differently than Na because it does not
565 necessarily just enter the cloud from below via updrafts, but rather it enters the cloud from above
566 via entrainment of air from the free troposphere that can at times be enriched with organic
567 species in the study region (Coggon et al., 2014; Crosbie et al., 2016; Hersey et al., 2009;
568 Sorooshian et al., 2007). For Fe, all turbulence scenarios yield a low correlation between Fe and
569 N_d, indicating that, overall, Fe is not a good predictor for N_d.

570   For Na, there is a better correlation at high turbulent conditions than at smooth conditions
571 ($R^2_{adj} = 0.26$ and $R^2_{adj} = 0.09$ for high and low σ_w, respectively). This further strengthens the
572 argument that turbulence plays an important role in the vertical transport of sea salt (and other
573 ocean emissions) from the ocean surface to the cloud base. The present data set allows for deeper
574 analysis into the entangled effects of sea salt and turbulence on N_d. More specifically, aerosol
575 reanalysis products like those from MERRA-2 calculate the mass concentration of sea salt via
576 parameterizations that link wind speed to sea salt emissions (Gong et al., 2003; Randles et al.,
577 2017). Since wind speed affects turbulence, it follows that sea salt concentrations are not
578 independent from turbulence, as turbulence is used to calculate sea salt concentrations.
579 Subsequently, these sea salt concentrations are used to predict N_d (e.g., McCoy et al., 2017,
580 2018). The present study measured both sea salt (quantified by Na) and turbulence (quantified by
581 σ_w) and thus offers an opportunity to try to isolate the effects of both factors on N_d (Figure 6).
582 Two results emerge. First, more turbulence is correlated to more sea salt, which is consistent
583 with what the models predict (Randles et al., 2017). Second, at a fixed concentration of Na, N_d
584 does not vary significantly with σ_w, as evidenced by a weak change in color. However, at a fixed
585 value of σ_w, N_d does vary significantly with Na, as evidenced by the noticeable change in color.
586 Therefore, the independent measurement of both variables reveals that N_d is more sensitive to
587 changes in Na than to changes in σ_w. We caution that σ_w is not obtained from below the cloud,
588 but from within the cloud during sampling time (Figure S1).

589

3.3.2. Effect of smoke influence

591   The clouds in the study region are affected by the smoke from wildfires (e.g., Dadashazar
592 et al., 2019; Maudlin et al., 2015; Schlosser et al., 2017). As mentioned in Section 2.7, Mardi et
593 al. (2018) used the same data set as this study and identified research flights (RFs) that contained
594 smoke-influenced cloud soundings, namely NiCE RFs 16–23 and FASE RFs 3–11 and 13–15. In
595 this study, we considered that all cloud water samples collected during the aforementioned RFs
596 were influenced by smoke. Furthermore, we did not distinguish if the smoke was above or below

in the cloud; this is an important caveat, as cloud microphysical properties seem to depend on the surrounding smoke vertical profile (e.g., Diamond et al, 2018; Koch & Del Genio, 2010). The correlation between N_d and composition as a function of smoke influence is shown in Figure 7 and Table 8, and the scatterplots from which the R^2_{adj} are taken are shown in Figure S4. Species that are produced during wildfires exhibited an improvement in R^2_{adj} when considering only the smoke-influenced cases. The opposite is true for species not produced during wildfires. More specifically, Ox and Fe showed an increase in correlation for smoke-influenced conditions (R^2_{adj} = 0.42 and R^2_{adj} = 0.15 for Ox and Fe, respectively) and a small decrease in for smoke-free conditions (R^2_{adj} = 0.07 and R^2_{adj} = 0.04 for Ox and Fe, respectively). This is most likely because Ox and Fe concentrations increase during wildfires (e.g., Maudlin et al., 2015) and thus contribute appreciably to the regional CCN during the summertime when wildfires are prevalent.

NSS-SO_4^{2-} and Na showed a decrease in correlation for smoke-influenced conditions (R^2_{adj} = 0.22 and R^2_{adj} = 0.17 for NSS-SO_4^{2-} and Na, respectively), and an increase for smoke-free conditions (R^2_{adj} = 0.36 and R^2_{adj} = 0.24 for NSS-SO_4^{2-} and Na, respectively). We suspect this is because even though wildfires can produce NSS-SO_4^{2-} (e.g., Reid et al., 1998) and Na (e.g., Hudson et al., 2004; Silva et al., 1999), these species are not produced as effectively as Ox or Fe. For example, Maudlin et al. (2015) measured aerosol mass concentration in the study region during both smoke-influenced and non-smoke-influenced conditions. They reported an increase in mass concentration for NSS-SO_4^{2-}, Na, Ox, and Fe to be 30%, 120%, 220%, and 408%, respectively, for submicron particles, and -2%, -28%, 164%, and 97%, respectively, for supermicrometer particles. Consequently, Ox and Fe are produced more in wildfires in the study region than NSS-SO_4^{2-} and Na.

The NiCE (2015) and FASE (2016) campaigns were influenced by smoke originating from different sources. NiCE was influenced by the Big Windy, Whiskey Complex, and Douglas Complex forest fires near the California-Oregon border, with a transport time of approximately two days to reach the base of aircraft operations in Marina and adjacent areas where most samples were collected (Maudlin et al., 2015). In contrast, FASE was influenced by the Soberanes fire approximately 30 km southwest of aircraft hangar (Braun et al., 2017). Hence, analyzing each campaign separately may provide some insights into the sensitivity of N_d to smoke from both different fuel types and with varying transport trajectories. NiCE fire data were linked to timber, grass and shrub models whereas those from FASE were associated with chaparral, tall grass, and timber (Braun et al., 2017; Mardi et al., 2018). The results are shown in Table 8 and Figure S4. When comparing FASE to both campaigns combined, the prediction of N_d using NSS-SO_4^{2-}, Na, Ox, and Fe is not improved, resulting in a ΔR^2_{adj} of -0.04, -0.04, 0.01, and -0.03, respectively. However, when comparing NiCE to both campaigns combined, the prediction of N_d using NSS-SO_4^{2-}, Na, Ox, and Fe is significantly improved, resulting in a ΔR^2_{adj} of 0.14, 0.29, 0.18, and 0.13, respectively. The difference between NiCE and FASE could be because different forest fires produce aerosols with varying aerosol chemical signatures and size distributions, as studies in the region have shown (Ma et al., 2019; Mardi et al., 2019). Alternatively, the difference could be due to the small sample size of NiCE (31 samples) as compared to FASE (136 samples) (Table 1). Certainly more research, including larger datasets, is warranted to investigate how different fuel types and plume aging times impact aerosol-cloud interactions.

3.3.3. Effect of in-cloud height

MacDonald et al. (2018) used the same data set as this study to show that the chemical composition of cloud water varies with height within a cloud. It is therefore reasonable that the N_d-chemical composition relationship also varies with in-cloud height. The correlation between N_d and composition as a dependence of in-cloud height is shown in Figure 8 and Table 8, and the scatterplots from which the R^2_{adj} are taken are shown in Figure S5.

Ox and Fe exhibit a better correlation when focusing on the bottom third of the cloud ($R^2_{adj} = 0.29$ and $R^2_{adj} = 0.20$ for Ox and Fe, respectively). When focusing on the top third of the cloud, the correlation decreased for Ox ($R^2_{adj} = 0.08$) and remained unchanged for Fe ($R^2_{adj} = 0.03$). One possible hypothesis to explain why Ox and Fe are better predictors of N_d at cloud base is that smokes affects cloud microphysics (N_d and effective radius) more at cloud base that at cloud top, regardless of whether the smoke was above or below the cloud (Diamond et al., 2018; Mardi et al., 2019).

NSS-SO$_4^{2-}$ and Na exhibit a better correlation with N_d when focusing on the top third of the cloud ($R^2_{adj} = 0.33$ and $R^2_{adj} = 0.33$ for NSS-SO$_4^{2-}$ and Na, respectively). The correlation decreases when focusing on the bottom third of the cloud ($R^2_{adj} = 0.17$ and $R^2_{adj} = 0.10$ for NSS-SO$_4^{2-}$ and Na, respectively). Tot-SO$_4^{2-}$ also follows this pattern ($R^2_{adj} = 0.56$ and $R^2_{adj} = 0.22$ for top and bottom, respectively).

It is not entirely clear why NSS-SO$_4^{2-}$ and Na would be better correlated with N_d in the top third of clouds. MacDonald et al. (2018) noted that the concentration of chemical species varies as a function of in-cloud height and is not the same for all species; the concentration of Na is greatest at cloud base whereas that of NSS-SO$_4^{2-}$ and Ox are greatest mid-cloud. It would be expected that the vertical profile of concentration is related to the ability to predict N_d (i.e., that a larger concentration of a species leads to a better correlation with N_d), but that expectation is not observed in these results. It is also interesting to point out that there is not much difference in R^2_{adj} when considering all cloud thirds versus only the middle third; this makes sense, as almost half of the cloud water samples (46%) were collected in the middle third of the cloud.

The dependence of the correlation between chemical composition and N_d on in-cloud height is of relevance to remote sensing, which relies on satellite measurement of cloud top properties such as cloud top temperature to then calculate a constant N_d throughout the cloud depth (e.g., Grosvenor et al., 2018).

4. Conclusions

This study used a four-year data set of airborne measurements collected in warm marine stratocumulus clouds off the California coast and analyzed the extent to which the chemical composition of cloud water can be used to predict N_d. A total of 80 species were filtered to nine to examine the prediction of N_d using a single-species model, and then using a multi-species model. The nine species were subsequently filtered to four to examine how the four single-species models were affected by environmental factors, namely, turbulence, smoke influence, and vertical location within a cloud. The most important findings of this paper are:

1. The species that best predicted N_d is Tot-SO$_4^{2-}$ with $R^2_{adj} = 0.40$, followed by NH$_4^+$ ($R^2_{adj} = 0.34$), NSS-SO$_4^{2-}$ ($R^2_{adj} = 0.29$), MSA ($R^2_{adj} = 0.26$), and NO$_3^-$ ($R^2_{adj} = 0.24$).
2. The prediction of N_d can be improved by using a multi-species model. However, increasing the number of species caused the R^2_{adj} to asymptotically approach ~ 0.6. Furthermore, the regressions with six or more species became statistically insignificant.

687   3. Analyzing the three best correlations for each of the n-species models (where n = 1–5) shows
688   that the factors that constitute a good regression are: a form of SO_4^{2-} (total or non-sea salt), an
689   ocean emissions tracer, and an organic tracer.
690   4. Greater turbulence (approximated as the standard deviation of vertical wind speed) improves
691   the ability of ocean-derived species to predict N_d, as observed when comparing regressions
692   using turbulent data points versus all data points for Tot-SO_4^{2-} (ΔR^2_{adj} = 0.15) and Na (ΔR^2_{adj}
693   = 0.07), but not for NSS-SO_4^{2-} (ΔR^2_{adj} = -0.01) or Ox (ΔR^2_{adj} = -0.06).
694   5. The influence of smoke significantly affects those species that best predict N_d. Ox (a species
695   known to be produced during biomass burning) was best correlated with N_d (R^2_{adj} = 0.42)
696   under smoke-influenced conditions.
697   6. Vertical location within the cloud affects the ability to predict N_d. The species that are best
698   correlated with N_d at cloud top are Tot-SO_4^{2-} (R^2_{adj} = 0.56) and NSS-SO_4^{2-} (R^2_{adj} = 0.33);
699   those best correlated with N_d at cloud base are fire tracers such as Ox (R^2_{adj} = 0.29) and Fe
700   (R^2_{adj} = 0.20), as it has been reported that the base of a cloud is more sensitive to the
701   influence of smoke.

Data Availability

All data used in this work can be found on the Figshare database (Sorooshian et al., 2017; https://figshare.com/articles/A_Multi-Year_Data_Set_on_Aerosol-Cloud-Precipitation-Meteorology_Interactions_for_Marine_Stratocumulus_Clouds/5099983).

Author Contributions

All coauthors contributed to some aspect of the data collection. ABM and AS conducted the data analysis and interpretation. ABM and AS prepared the manuscript with contributions from all coauthors.

Competing Interests

The authors declare that they have no conflict of interest.

Acknowledgements

Alexander B. MacDonald acknowledges support from the Mexican National Council for Science and Technology (CONACYT). We acknowledge Agilent Technologies for their support and Shane Snyder's laboratories for ICP-QQQ data.

Financial Support

These field campaigns were funded by Office of Naval Research grants N00014-10-1-0811, N00014-11-1-0783, N00014-10-1-0200, N00014-04-1-0118, and N00014-16-1-2567. This work was also partially supported by NASA grant 80NSSC19K0442 in support of the ACTIVATE Earth Venture Suborbital-3 (EVS-3) investigation, which is funded by NASA's Earth Science Division and managed through the Earth System Science Pathfinder Program Office.

References

Abdul-Razzak, H. and Ghan, S. J.: A parameterization of aerosol activation 2. Multiple aerosol types, J. Geophys. Res., 105(D5), 6837–6844, https://doi.org/10.1029/1999JD901161, 2000.

Ackerman, A. S., Kirkpatrick, M. P., Stevens, D. E., and Toon, O. B.: The impact of humidity above stratiform clouds on indirect aerosol climate forcing, Nature, 432(7020), 1014–1017, https://doi.org/10.1038/nature03174, 2004.

Adams, P. J. and Seinfeld, J. H.: Disproportionate impact of particulate emissions on global cloud condensation nuclei concentrations, Geophys. Res. Lett., 30(5), 1239, https://doi.org/10.1029/2002gl016303, 2003.

Albrecht, B. A.: Aerosols, Cloud Microphysics, and Fractional Cloudiness, Science, 245(4923), 1227–1230, https://doi.org/10.1126/science.245.4923.1227, 1989.

Andreae, M. O. and Rosenfeld, D.: Aerosol-cloud-precipitation interactions. Part 1. The nature and sources of cloud-active aerosols, Earth-Science Rev., 89(1–2), 13–41, https://doi.org/10.1016/j.earscirev.2008.03.001, 2008.

ApSimon, H. M., Kruse, M. and Bell, J. N. B.: Ammonia emissions and their role in acid deposition, Atmos. Environ., 21(9), 1939–1946, https://doi.org/10.1016/0004-6981(87)90154-5, 1987.

Bauer, S. E., Tsigaridis, K. and Miller, R.: Significant atmospheric aerosol pollution caused by world food cultivation, Geophys. Res. Lett., 43(10), 5394–5400, https://doi.org/10.1002/2016GL068354, 2016.

Baumgardner, D., Jonsson, H., Dawson, W., O'Connor, D. and Newton, R.: The cloud, aerosol and precipitation spectrometer: A new instrument for cloud investigations, Atmos. Res., 59–60, 251–264, https://doi.org/10.1016/S0169-8095(01)00119-3, 2001.

Behrenfeld, M. J., Moore, R. H., Hostetler, C. A., Graff, J., Gaube, P., Russell, L. M., Chen, G., Doney, S. C., Giovannoni, S., Liu, H., Proctor, C., Bolaños, L. M., Baetge, N., Davie-Martin, C., Westberry, T. K., Bates, T. S., Bell, T. G., Bidle, K. D., Boss, E. S., Brooks, S. D., Cairns, B., Carlson, C., Halsey, K., Harvey, E. L., Hu, C., Karp-Boss, L., Kleb, M., Menden-Deuer, S., Morison, F., Quinn, P. K., Scarino, A. J., Anderson, B., Chowdhary, J., Crosbie, E., Ferrare, R., Hair, J. W., Hu, Y., Janz, S., Redemann, J., Saltzman, E., Shook, M., Siegel, D. A., Wisthaler, A., Martin, M. Y. and Ziemba, L.: The North Atlantic Aerosol and Marine Ecosystem Study (NAAMES): Science motive and mission overview, Front. Mar. Sci., 6, 1–25, https://doi.org/10.3389/fmars.2019.00122, 2019.

Bellouin, N., Quaas, J., Gryspeerdt, E., Kinne, S., Stier, P., Watson-Parris, D., Boucher, O., Carslaw, K. S., Christensen, M., Daniau, A.-L., Dufresne, J.-L., Feingold, G., Fiedler, S., Forster, P., Gettelman, A., Haywood, J. M., Lohmann, U., Malavelle, F., Mauritsen, T., McCoy, D. T., Myhre, G., Mülmenstädt, J., Neubauer, D., Possner, A., Rugenstein, M., Sato, Y., Schulz, M., Schwartz, S. E., Sourdeval, O., Storelvmo, T., Toll, V., Winker, D., and Stevens, B.: Bounding Global Aerosol Radiative Forcing of Climate Change, Rev. Geophys., 58, e2019RG000660, https://doi.org/10.1029/2019rg000660, 2020.

Borys, R. D., Lowenthal, D. H., Wetzel, M. A., Herrera, F., Gonzalez, A. and Harris, J.: Chemical and microphysical properties of marine stratiform cloud in the North Atlantic, J. Geophys. Res. Atmos., 103(D17), 22073–22085, https://doi.org/10.1029/98JD02087, 1998.

Boucher, O. and Lohmann, U.: The sulfate-CCN-cloud albedo effect, Tellus B Chem. Phys. Meteorol., 47(3), 281–300, https://doi.org/10.3402/tellusb.v47i3.16048, 1995.

775 Bouwman, A. F., Lee, D. S., Asman, W. A. H., Dentener, F. J., Van Der Hoek, K. W. and
776   Olivier, J. G. J.: A global high-resolution emission inventory for ammonia, Global
777   Biogeochem. Cycles, 11(4), 561–587, https://doi.org/10.1029/97GB02266, 1997.
778 Charlson, R. J., Lovelockt, J. E., Andreae, M. O. and Warren, S. G.: Oceanic phytoplankton,
779   atmospheric sulphur, cloud albedo and climate, Nature, 326(6114), 655–661,
780   https://doi.org/10.1038/326655a0, 1987.
781 Charlson, R. J., Schwartz, S. E., Hales, J. M., Cess, R. D., Coakley, J. J., Hansen, J. E. and
782   Hofmann, D. J.: Climate forcing by anthropogenic aerosols, Science, 117(5043), 423–430,
783   https://doi.org/10.1126/science.255.5043.423, 1992.
784 Chen, Y. and Penner, J. E.: Uncertainty analysis for estimates of the first indirect aerosol effect,
785   Atmos. Chem. Phys., 5(11), 2935–2948, https://doi.org/10.5194/acp-5-2935-2005, 2005.
786 Chen, Y.-C., Christensen, M. W., Xue, L., Sorooshian, A., Stephens, G. L., Rasmussen, R. M.
787   and Seinfeld, J. H.: Occurrence of lower cloud albedo in ship tracks, Atmos. Chem. Phys.,
788   12(17), 8223–8235, https://doi.org/10.5194/acp-12-8223-2012, 2012.
789 Chuang, C. C., Penner, J. E. and Edwards, L. L.: Nucleation Scavenging of Smoke Particles and
790   Simulated Drop Size Distributions over Large Biomass Fires, J. Atmos. Sci., 49(14),
791   1264–1276, https://doi.org/10.1175/1520-0469(1992)049<1264:NSOSPA>2.0.CO;2,
792   1992.
793 Chuang, C. C. and Penner, J. E.: Effects of anthropogenic sulfate on cloud drop nucleation and
794   optical properties, Tellus B Chem. Phys. Meteorol., 47(5), 566–577,
795   https://doi.org/10.1034/j.1600-0889.47.issue5.4.x, 1995.
796 Coggon, M. M., Sorooshian, A., Wang, Z., Metcalf, A. R., Frossard, A. A., Lin, J. J., Craven, J.
797   S., Nenes, A., Jonsson, H. H., Russell, L. M., Flagan, R. C. and Seinfeld, J. H.: Ship
798   impacts on the marine atmosphere: Insights into the contribution of shipping emissions to
799   the properties of marine aerosol and clouds, Atmos. Chem. Phys., 12(18), 8439–8458,
800   https://doi.org/10.5194/acp-12-8439-2012, 2012.
801 Coggon, M. M., Sorooshian, A., Wang, Z., Craven, J. S., Metcalf, A. R., Lin, J. J., Nenes, A.,
802   Jonsson, H. H., Flagan, R. C. and Seinfeld, J. H.: Observations of continental biogenic
803   impacts on marine aerosol and clouds off the coast of California, J. Geophys. Res. Atmos.,
804   119(11), 6724–6748, https://doi.org/10.1002/2013JD021228, 2014.
805 Crosbie, E., Wang, Z., Sorooshian, A., Chuang, P. Y., Craven, J. S., Coggon, M. M., Brunke, M.,
806   Zeng, X., Jonsson, H., Woods, R. K., Flagan, R. C. and Seinfeld, J. H.: Stratocumulus
807   Cloud Clearings and Notable Thermodynamic and Aerosol Contrasts across the Clear–
808   Cloudy Interface, J. Atmos. Sci., 73(3), 1083–1099, https://doi.org/10.1175/JAS-D-15-
809   0137.1, 2016.
810 Dadashazar, H., Wang, Z., Crosbie, E., Brunke, M., Zeng, X., Jonsson, H., Woods, R. K.,
811   Flagan, R. C., Seinfeld, J. H. and Sorooshian, A.: Relationships between giant sea salt
812   particles and clouds inferred from aircraft physicochemical data, J. Geophys. Res., 122(6),
813   3421–3434, https://doi.org/10.1002/2016JD026019, 2017.
814 Dadashazar, H., Ma, L. and Sorooshian, A.: Sources of pollution and interrelationships between
815   aerosol and precipitation chemistry at a central California site, Sci. Total Environ., 651,
816   1776–1787, https://doi.org/10.1016/j.scitotenv.2018.10.086, 2019.
817 Diamond, M. S., Dobracki, A., Freitag, S., Griswold, J. D. S., Heikkila, A., Howell, S. G.,
818   Kacarab, M. E., Podolske, J. R., Saide, P. E. and Wood, R.: Time-dependent entrainment
819   of smoke presents an observational challenge for assessing aerosol-cloud interactions over

820   the southeast Atlantic Ocean, Atmos. Chem. Phys., 18(19), 14623–14636,
821   https://doi.org/10.5194/acp-18-14623-2018, 2018.

822 Facchini, M. C., Mircea, M., Fuzzi, S. and Charlson, R. J.: Cloud albedo enhancement by
823   surface-active organic solutes in growing droplets, Nature, 401(6750), 257–259,
824   https://doi.org/10.1038/45758, 1999.

825 Feingold, G., Frisch, A. S., Stevens, B. and Cotton, W. R.: On the relationship among cloud
826   turbulence, droplet formation and drizzle as viewed by Doppler radar, microwave
827   radiometer and lidar, J. Geophys. Res. Atmos., 104(D18), 22195–22203,
828   https://doi.org/10.1029/1999JD900482, 1999.

829 Feingold, G., Cotton, W. R., Kreidenweis, S. M. and Davis, J. T.: The Impact of Giant Cloud
830   Condensation Nuclei on Drizzle Formation in Stratocumulus: Implications for Cloud
831   Radiative Properties, J. Atmos. Sci., 56, 4100–4117, http://doi.org/10.1175/1520-
832   0469(1999)056<4100:TIOGCC>2.0.CO;2, 1999.

833 Fountoukis, C. and Nenes, A.: Continued development of a cloud droplet formation
834   parameterization for global climate models, J. Geophys. Res. Atmos., 110(D11), D11212,
835   https://doi.org/10.1029/2004JD005591, 2005.

836 Freund, R. J., Wilson, W. J. and Mohr, D. L.: Statistical Methods, 3rd ed., Academic Press,
837   Burlington, MA., 2010.

838 Gelaro, R., McCarty, W., Suárez, M. J., Todling, R., Molod, A., Takacs, L., Randles, C. A.,
839   Darmenov, A., Bosilovich, M. G., Reichle, R., Wargan, K., Coy, L., Cullather, R., Draper,
840   C., Akella, S., Buchard, V., Conaty, A., da Silva, A. M., Gu, W., Kim, G. K., Koster, R.,
841   Lucchesi, R., Merkova, D., Nielsen, J. E., Partyka, G., Pawson, S., Putman, W.,
842   Rienecker, M., Schubert, S. D., Sienkiewicz, M. and Zhao, B.: The modern-era
843   retrospective analysis for research and applications, version 2 (MERRA-2), J. Clim.,
844   30(14), 5419–5454, https://doi.org/10.1175/JCLI-D-16-0758.1, 2017.

845 Gerber, H., Arends, B. G. and Ackerman, A. S.: New microphysics sensor for aircraft use,
846   Atmos. Res., 31(4), 235–252, https://doi.org/10.1016/0169-8095(94)90001-9, 1994.

847 Gerber, H., Frick, G. and Rodi, A. R.: Ground-based FSSP and PVM measurements of liquid
848   water content, J. Atmos. Ocean. Technol., 16(8), 1143–1149,
849   https://doi.org/10.1175/1520-0426(1999)016<1143:GBFAPM>2.0.CO;2, 1999.

850 Ghan, S. J., Leung, L. R. and Easter, R. C.: Prediction of cloud droplet number in a general
851   circulation model, J. Geophys. Res., 102(D18), 21777–21794,
852   https://doi.org/10.1029/97JD01810, 1997.

853 Ghan, S. J., Abdul-Razzak, H., Nenes, A., Ming, Y., Liu, X., Ovchinnikov, M., Shipway, B.,
854   Meskhidze, N., Xu, J. and Shi, X.: Droplet nucleation: Physically-based parameterizations
855   and comparative evaluation, J. Adv. Model. Earth Syst., 3(4), 1–34,
856   https://doi.org/10.1029/2011ms000074, 2011.

857 Gong, S. L.: A parameterization of sea-salt aerosol source function for sub- and super-micron
858   particles, Global Biogeochem. Cycles, 17(4), 1097, https://doi.org/2003gb002079, 2003.

859 Grosvenor, D. P., Sourdeval, O., Zuidema, P., Ackerman, A., Alexandrov, M. D., Bennartz, R.,
860   Boers, R., Cairns, B., Chiu, J. C., Christensen, M., Deneke, H., Diamond, M., Feingold,
861   G., Fridlind, A., Hünerbein, A., Knist, C., Kollias, P., Marshak, A., McCoy, D., Merk, D.,
862   Painemal, D., Rausch, J., Rosenfeld, D., Russchenberg, H., Seifert, P., Sinclair, K., Stier,
863   P., van Diedenhoven, B., Wendisch, M., Werner, F., Wood, R., Zhang, Z. and Quaas, J.:
864   Remote Sensing of Droplet Number Concentration in Warm Clouds: A Review of the

865   Current State of Knowledge and Perspectives, Rev. Geophys., 56(2), 409–453,
866   https://doi.org/10.1029/2017RG000593, 2018.
867 Hegg, D. A.: Impact of gas-phase HNO3 and NH3 on microphysical processes in atmospheric
868   clouds, Geophys. Res. Lett., 27(15), 2201–2204, https://doi.org/10.1029/1999GL011252,
869   2000.
870 Hegg, D. A. and Hobbs, P. V.: Cloud Water Chemistry and the production of sulfates in clouds,
871   Atmos. Environ., 15(9), 1597–1604, https://doi.org/10.1016/0004-6981(81)90144-X,
872   1981.
873 Hegg, D. A. and Hobbs, P. V.: Sulfate and nitrate chemistry in cumuliform clouds, Atmos.
874   Environ., 20(5), 901–909, https://doi.org/10.1016/0004-6981(86)90274-X, 1986.
875 Hegg, D. A., Ferek, R. J. and Hobbs, P. V.: Light scattering and cloud condensation nucleus
876   activity of sulfate aerosol measured over the northeast Atlantic Ocean, J. Geophys. Res.
877   Atmos., 98(D8), 14887–14894, https://doi.org/10.1029/93JD01615, 1993.
878 Hersey, S. P., Sorooshian, A., Murphy, S. M., Flagan, R. C. and Seinfeld, J. H.: Aerosol
879   hygroscopicity in the marine atmosphere: a closure study using high-resolution, size-
880   resolved AMS and multiple-RH DASH-SP data, Atmos. Chem. Phys., 9(7), 16789–16817,
881   https://doi.org/10.5194/acpd-8-16789-2008, 2009.
882 Hudson, P. K., Murphy, D. M., Cziczo, D. J., Thomson, D. S., de Gouw, J. A., Warneke, C.,
883   Holloway, J., Jost, H. J. and Hübler, G.: Biomass-burning particle measurements:
884   Characteristics composition and chemical processing, J. Geophys. Res. Atmos., 109,
885   D23S27, https://doi.org/10.1029/2003JD004398, 2004.
886 Intergovernmental Panel on Climate Change: Climate Change 2007: The Physical Science Basis.
887   Contribution of Working Group I to the Fourth Assessment Report of the
888   Intergovernmental Panel on Climate Change, Cambridge University Press, Cambridge,
889   United Kingdom and New York, NY, USA., 2007.
890 Intergovernmental Panel on Climate Change: Climate Change 2013: The Physical Science Basis.
891   Contribution of Working Group I to the Fifth Assessment Report of the Intergovernmental
892   Panel on Climate Change, Cambridge University Press, Cambridge, United Kingdom and
893   New York, NY, USA., 2013.
894 Jung, E., Albrecht, B. A., Jonsson, H. H., Chen, Y.-C., Seinfeld, J. H., Sorooshian, A., Metcalf,
895   A. R., Song, S., Fang, M. and Russell, L. M.: Precipitation effects of giant cloud
896   condensation nuclei artificially introduced into stratocumulus clouds, Atmos. Chem.
897   Phys., 15, 5645–5658, http://doi.org/10.5194/acp-15-5645-2015, 2015.
898 Jickells, T. D., An, Z. S., Andersen, K. K., Baker, A. R., Bergametti, G., Brooks, N., Cao, J. J.,
899   Boyd, P. W., Duce, R. A., Hunter, K. A., Kawahata, H., Kubilay, N. and Liss, P. S.:
900   Global Iron Connections Between Desert Dust, Ocean Biogeochemistry, and Climate,
901   Science, 308(5718), 67–71, https://doi.org/10.1126/science.1105959, 2005.
902 Kahane, L. H.: Regression Basics, 2nd ed., Sage Publications, Thousand Oaks, CA., 2008.
903 Koch, D. and Del Genio, A. D.: Black carbon semi-direct effects on cloud cover: Review and
904   synthesis, Atmos. Chem. Phys., 10(16), 7685–7696, https://doi.org/10.5194/acp-10-7685-
905   2010, 2010.
906 Kulmala, M., Laaksonen, A., Korhonen, P., Vesala, T., Ahonen, T. and Barrett, J. C.: The effect
907   of atmospheric nitric acid vapor on cloud condensation nucleus activation, J. Geophys.
908   Res., 98(D12), 22949–22958, https://doi.org/10.1029/93JD02070, 1993.
909 Lance, S., Nenes, A., Mazzoleni, C., Dubey, M. K., Gates, H., Varutbangkul, V., Rissman, T. A.,
910   Murphy, S. M., Sorooshian, A., Flagan, R. C., Seinfeld, J. H., Feingold, G. and Jonsson,

911   H. H.: Cloud condensation nuclei activity, closure, and droplet growth kinetics of Houston
912   aerosol during the Gulf of Mexico Atmospheric Composition and Climate Study
913   (GoMACCS), J. Geophys. Res., 114, D00F15, https://doi.org/10.1029/2008jd011699,
914   2009.
915   Leaitch, W. R., Strapp, J. W., Wiebe, H. A., Anlauf, K. G. and Isaac, G. A.: Chemical and
916   microphysical studies of nonprecipitating summer cloud in Ontario, Canada, J. Geophys.
917   Res. Atmos., 91(D11), 11821–11831, https://doi.org/10.1029/JD091iD11p11821, 1986.
918   Leaitch, W. R., Isaac, G. A., Strapp, J. W., Banic, C. M. and Wiebe, H. A.: The relationship
919   between cloud droplet number concentrations and anthropogenic pollution: observations
920   and climatic implications, J. Geophys. Res. Atmos., 97(D2), 2463–2474,
921   https://doi.org/10.1029/91JD02739, 1992.
922   Leaitch, W. R., Banic, C. M., Isaac, G. A., Couture, M. D., Liu, P. S. K., Gultepe, I., Li, S. M.,
923   Kleinman, L., Daum, P. H. and MacPherson, J. I.: Physical and chemical observations in
924   marine stratus during the 1993 North Atlantic Regional Experiment: Factors controlling
925   cloud droplet number concentrations, J. Geophys. Res. Atmos., 101(D22), 29123–29135,
926   https://doi.org/10.1029/96JD01228, 1996.
927   Lowenthal, D. H. and Borys, R. D.: Sources of microphysical variation in marine stratiform
928   clouds in the North Atlantic, Geophys. Res. Lett., 27(10), 1491–1494,
929   https://doi.org/10.1029/1999GL010992, 2000.
930   Lowenthal, D. H., Borys, R. D., Choularton, T. W., Bower, K. N., Flynn, M. J. and Gallagher,
931   M. W.: Parameterization of the cloud droplet–sulfate relationship, Atmos. Environ., 38(2),
932   287–292, https://doi.org/10.1016/j.atmosenv.2003.09.046, 2004.
933   Lu, M. L., Sorooshian, A., Jonsson, H. H., Feingold, G., Flagan, R. C. and Seinfeld, J. H.:
934   Marine stratocumulus aerosol-cloud relationships in the MASE-II experiment:
935   Precipitation susceptibility in eastern Pacific marine stratocumulus, J. Geophys. Res.
936   Atmos., 114(24), 1–11, https://doi.org/10.1029/2009JD012774, 2009.
937   Ma, L., Dadashazar, H., Braun, R. A., MacDonald, A. B., Aghdam, M. A., Maudlin, L. C. and
938   Sorooshian, A.: Size-resolved characteristics of water-soluble particulate elements in a
939   coastal area: Source identification, influence of wildfires, and diurnal variability, Atmos.
940   Environ., 206, 72–84, https://doi.org/10.1016/j.atmosenv.2019.02.045, 2019.
941   MacDonald, A. B., Dadashazar, H., Chuang, P. Y., Crosbie, E., Wang, H., Wang, Z., Jonsson, H.
942   H., Flagan, R. C., Seinfeld, J. H. and Sorooshian, A.: Characteristic Vertical Profiles of
943   Cloud Water Composition in Marine Stratocumulus Clouds and Relationships with
944   Precipitation, J. Geophys. Res. Atmos., 123(7), 3704–3723,
945   https://doi.org/10.1002/2017JD027900, 2018.
946   Mardi, A. H., Dadashazar, H., MacDonald, A. B., Braun, R. A., Crosbie, E., Xian, P., Thorsen,
947   T. J., Coggon, M. M., Fenn, M. A., Ferrare, R. A., Hair, J. W., Woods, R. K., Jonsson, H.
948   H., Flagan, R. C., Seinfeld, J. H. and Sorooshian, A.: Biomass Burning Plumes in the
949   Vicinity of the California Coast: Airborne Characterization of Physicochemical Properties,
950   Heating Rates, and Spatiotemporal Features, J. Geophys. Res. Atmos., 123(23), 13560–
951   13582, https://doi.org/10.1029/2018JD029134, 2018.
952   Mardi, A. H., Dadashazar, H., MacDonald, A. B., Crosbie, E., Coggon, M. M., Aghdam, M. A.,
953   Woods, R. K., Jonsson, H. H., Flagan, R. C., Seinfeld, J. H. and Sorooshian, A.: Effects of
954   Biomass Burning on Stratocumulus Droplet Characteristics, Drizzle Rate, and
955   Composition, J. Geophys. Res. Atmos., 124(22), 12301–12318,
956   https://doi.org/10.1029/2019JD031159, 2019.

Matsumoto, K., Tanaka, H., Nagao, I. and Ishizaka, Y.: Contribution of particulate sulfate and organic carbon to cloud condensation nuclei in the marine atmosphere, Geophys. Res. Lett., 24(6), 655–658, https://doi.org/10.1029/97GL00541, 1997.

Maudlin, L. C., Wang, Z., Jonsson, H. H. and Sorooshian, A.: Impact of wildfires on size-resolved aerosol composition at a coastal California site, Atmos. Environ., 119, 59–68, https://doi.org/10.1016/j.atmosenv.2015.08.039, 2015.

McCoy, D. T., Bender, F. A.-M., Mohrmann, J. K. C., Hartmann, D. L., Wood, R. and Grosvenor, D. P.: The global aerosol-cloud first indirect effect estimated using MODIS, MERRA, and AeroCom, J. Geophys. Res. Atmos., 122(3), 1779–1796, https://doi.org/10.1002/2016JD026141, 2017.

McCoy, D. T., Bender, F. A.-M., Grosvenor, D. P., Mohrmann, J. K., Hartmann, D. L., Wood, R. and Field, P. R.: Predicting decadal trends in cloud droplet number concentration using reanalysis and satellite data, Atmos. Chem. Phys., 18(3), 2035–2047, https://doi.org/10.5194/acp-18-2035-2018, 2018.

Medina, J., Nenes, A., Sotiropoulou, R. E. P., Cottrell, L. D., Ziemba, L. D., Beckman, P. J. and Griffin, R. J.: Cloud condensation nuclei closure during the International Consortium for Atmospheric Research on Transport and Transformation 2004 campaign: Effects of size-resolved composition, J. Geophys. Res. Atmos., 112(D10), D10S31, https://doi.org/10.1029/2006JD007588, 2007.

Menon, S. and Saxena, V. K.: Role of sulfates in regional cloud–climate interactions, Atmos. Res., 47–48, 299–315, https://doi.org/https://doi.org/10.1016/S0169-8095(98)00057-X, 1998.

Menon, S., Genio, A. D. Del, Koch, D. and Tselioudis, G.: GCM Simulations of the Aerosol Indirect Effect: Sensitivity to Cloud Parameterization and Aerosol Burden, J. Atmos. Sci., 59(3), 692–713, https://doi.org/10.1175/1520-0469(2002)059<0692:gsotai>2.0.co;2, 2002.

Nenes, A., Charlson, R. J., Facchini, M. C., Kulmala, M., Laaksonen, A. and Seinfeld, J. H.: Can chemical effects on cloud droplet number rival the first indirect effect?, Geophys. Res. Lett., 29(17), 1848, https://doi.org/10.1029/2002gl015295, 2002.

Nenes, A. and Seinfeld, J. H.: Parameterization of cloud droplet formation in global climate models, J. Geophys. Res. Atmos., 108(D14), 1–14, https://doi.org/10.1029/2002jd002911, 2003.

Novakov, T. and Penner, J. E.: Large contribution of organic aerosols to cloud-condensation-nuclei concentrations, Nature, 365(6449), 823–826, https://doi.org/10.1038/365823a0, 1993.

Novakov, T., Rivera-Carpio, C., Penner, J. E. and Rogers, C. F.: The effect of anthropogenic sulfate aerosols on marine cloud droplet concentrations, Tellus B Chem. Phys. Meteorol., 46(2), 132–141, https://doi.org/10.3402/tellusb.v46i2.15758, 1994.

Partridge, D. G., Vrugt, J. A., Tunved, P., Ekman, A. M. L., Struthers, H. and Sorooshian, A.: Inverse modelling of cloud-aerosol interactions - Part 2: Sensitivity tests on liquid phase clouds using a Markov chain Monte Carlo based simulation approach, Atmos. Chem. Phys., 12(6), 2823–2847, https://doi.org/10.5194/acp-12-2823-2012, 2012.

Paulot, F., Jacob, D. J., Johnson, M. T., Bell, T. G., Baker, A. R., Keene, W. C., Lima, I. D., Doney, S. C. and Stock, C. A.: Global oceanic emission of ammonia: Constraints from seawater and atmospheric observations, Global Biogeochem. Cycles, 29(8), 1165–1178, https://doi.org/10.1002/2015GB005106, 2015.

1003   Prabhakar, G., Ervens, B., Wang, Z., Maudlin, L. C., Coggon, M. M., Jonsson, H. H., Seinfeld, J.
1004   H. and Sorooshian, A.: Sources of nitrate in stratocumulus cloud water: Airborne
1005   measurements during the 2011 E-PEACE and 2013 NiCE studies, Atmos. Environ., 97,
1006   166–173, https://doi.org/10.1016/j.atmosenv.2014.08.019, 2014.
1007   Pringle, K. J., Carslaw, K. S., Spracklen, D. V., Mann, G. M. and Chipperfield, M. P.: The
1008   relationship between aerosol and cloud drop number concentrations in a global aerosol
1009   microphysics model, Atmos. Chem. Phys., 9(12), 4131–4144, https://doi.org/10.5194/acp-
1010   9-4131-2009, 2009.
1011   Pueschel, R. F., Valin, C. C., Castillo, R. C., Kadlecek, J. A. and Ganor, E.: Aerosols in polluted
1012   versus nonpolluted air masses: long-range transport and effects on clouds, J. Appl.
1013   Meteorol. Clim., 25, 1908–1917, https://doi.org/10.1175/1520-
1014   0450(1986)025<1908:AIPVNA>2.0.CO;2, 1986.
1015   Pye, H. O. T., Nenes, A., Alexander, B., Ault, A. P., Barth, M. C., Clegg, S. L., Collett Jr., J. L.,
1016   Fahey, K. M., Hennigan, C. J., Herrmann, H., Kanakidou, M., Kelly, J. T., Ku, I.-T.,
1017   McNeill, V. F., Riemer, N., Schaefer, T., Shi, G., Tilgner, A., Walker, J. T., Wang, T.,
1018   Weber, R., Xing, J., Zaveri, R. A. and Zuend, A.: The acidity of atmospheric particles and
1019   clouds, Atmos. Chem. Phys., 20(8), 4809–4888, , https://doi.org/10.5194/acp-20-4809-
1020   2020, 2020.
1021   Quinn, P. K., Coffman, D. J., Johnson, J. E., Upchurch, L. M. and Bates, T. S.: Small fraction of
1022   marine cloud condensation nuclei made up of sea spray aerosol, Nat. Geosci., 10(9), 674–
1023   679, https://doi.org/10.1038/ngeo3003, 2017.
1024   Randles, C. A., da Silva, A. M., Buchard, V., Colarco, P. R., Darmenov, A., Govindaraju, R.,
1025   Smirnov, A., Holben, B., Ferrare, R., Hair, J., Shinozuka, Y. and Flynn, C. J.: The
1026   MERRA-2 aerosol reanalysis, 1980 onward. Part I: System description and data
1027   assimilation evaluation, J. Clim., 30(17), 6823–6850, https://doi.org/10.1175/JCLI-D-16-
1028   0609.1, 2017.
1029   Reid, J. S., Hobbs, P. V., Ferek, R. J., Blake, D. R., Martins, J. V., Dunlap, M. R. and Liousse,
1030   C.: Physical, chemical, and optical properties of regional hazes dominated by smoke in
1031   Brazil, J. Geophys. Res. Atmos., 103(D24), 32059–32080,
1032   https://doi.org/10.1029/98JD00458, 1998.
1033   Russell, L. M., Sorooshian, A., Seinfeld, J. H., Albrecht, B. A., Nenes, A., Ahlm, L., Chen, Y.-
1034   C., Coggon, M., Craven, J. S., Flagan, R. C., Frossard, A. A., Jonsson, H., Jung, E., Lin, J.
1035   J., Metcalf, A. R., Modini, R., Mülmenstädt, J., Roberts, G. C., Shingler, T., Song, S.,
1036   Wang, Z. and Wonaschütz, A.: Eastern pacific emitted aerosol cloud experiment, Bull.
1037   Am. Meteorol. Soc., 94(5), 709–729, https://doi.org/10.1175/BAMS-D-12-00015.1, 2013.
1038   Saxena, V. K. and Menon, S.: Sulfate-induced cooling in the southeastern US: An observational
1039   assessment, Geophys. Res. Lett., 26(16), 2489–2492,
1040   https://doi.org/10.1029/1999GL900555, 1999.
1041   Schlosser, J. S., Braun, R. A., Bradley, T., Dadashazar, H., MacDonald, A. B., Aldhaif, A. A.,
1042   Azadi Aghdam, M., Hossein Mardi, A., Xian, P. and Sorooshian, A.: Analysis of Aerosol
1043   Composition Data for Western United States Wildfires Between 2005-2015: Dust
1044   Emissions, Chloride Depletion, and Most Enhanced Aerosol Constituents, J. Geophys.
1045   Res. Atmos., 122(16), 8951–8966, https://doi.org/10.1002/2017JD026547, 2017.
1046   Schlosser, J. S., Dadashazar, H., Edwards, E.-L., Mardi, A. H., Prabhakar, G., Stahl, C., Jonsson,
1047   H. H. and Sorooshian, A.: Relationships between supermicrometer sea salt aerosol and

1048   marine boundary layer conditions: insights from repeated identical flight patterns, J.
1049   Geophys. Res. Atmos., accepted, https://doi.org/10.1029/2019JD032346, 2020.
1050 Seinfeld, J. H. and Pandis, S. N.: Atmospheric Chemistry and Physics, 3rd ed., New York, NY.,
1051   2016.
1052 Silva, P. J., Liu, D. Y., Noble, C. A. and Prather, K. A.: Size and chemical characterization of
1053   individual particles resulting from biomass burning of local Southern California species,
1054   Environ. Sci. Technol., 33(18), 3068–3076, https://doi.org/10.1021/es980544p, 1999.
1055 Sorooshian, A., Lu, M. L., Brechtel, F. J., Jonsson, H., Feingold, G., Flagan, R. C. and Seinfeld,
1056   J. H.: On the source of organic acid aerosol layers above clouds, Environ. Sci. Technol.,
1057   41(13), 4647–4654, https://doi.org/10.1021/es0630442, 2007.
1058 Sorooshian, A., Padró, L. T., Nenes, A., Feingold, G., McComiskey, A., Hersey, S. P., Gates, H.,
1059   Jonsson, H. H., Miller, S. D., Stephens, G. L., Flagan, R. C. and Seinfeld, J. H.: On the
1060   link between ocean biota emissions, aerosol, and maritime clouds: Airborne, ground, and
1061   satellite measurements off the coast of California, Global Biogeochem. Cycles, 23(4), 1–
1062   15, https://doi.org/10.1029/2009GB003464, 2009.
1063 Sorooshian, A., MacDonald, A. B., Dadashazar, H., Bates, K. H., Coggon, M. M., Craven, J. S.,
1064   Crosbie, E., Edwards, E.-L., Hersey, S. P., Hodas, N., Lin, J. J., Hossein Mardi, A., Marty,
1065   A. N., Maudlin, L. C., Metcalf, A. R., Murphy, S. M., Padro, L. T., Prabhakar, G.,
1066   Rissman, T. A., Schlosser, J., Shingler, T., Varutbangkul, V., Wang, Z., Woods, R. K.,
1067   Chuang, P. Y., Nenes, A., Jonsson, H. H., Flagan, R. C. and Seinfeld, J. H.: A multi-year
1068   data set on aerosol-cloud-precipitation-meteorology interactions for marine stratocumulus
1069   clouds, figshare, https://doi.org/10.6084/m9.figshare.5099983.v10, 2017.
1070 Sorooshian, A., MacDonald, A. B., Dadashazar, H., Bates, K. H., Coggon, M. M., Craven, J. S.,
1071   Crosbie, E., Hersey, S. P., Hodas, N., Lin, J. J., Negrón Marty, A., Maudlin, L. C.,
1072   Metcalf, A. R., Murphy, S. M., Padró, L. T., Prabhakar, G., Rissman, T. A., Shingler, T.,
1073   Varutbangkul, V., Wang, Z., Woods, R. K., Chuang, P. Y., Nenes, A., Jonsson, H. H.,
1074   Flagan, R. C. and Seinfeld, J. H.: A multi-year data set on aerosol-cloud-precipitation-
1075   meteorology interactions for marine stratocumulus clouds, Sci. Data, 5, 1–13,
1076   https://doi.org/10.1038/sdata.2018.26, 2018.
1077 Sorooshian, A., Anderson, B., Bauer, S. E., Braun, R. A., Cairns, B., Crosbie, E., Dadashazar,
1078   H., Diskin, G., Ferrare, R., Flagan, R. C., Hair, J., Hostetler, C., Jonsson, H. H., Kleb, M.
1079   M., Liu, H., Macdonald, A. B., McComiskey, A., Moore, R., Painemal, D., Russell, L. M.,
1080   Seinfeld, J. H., Shook, M., Smith, W. L., Thornhill, K., Tselioudis, G., Wang, H., Zeng,
1081   X., Zhang, B., Ziemba, L. and Zuidema, P.: Aerosol–cloud–meteorology interaction
1082   airborne field investigations: Using lessons learned from the U.S. West coast in the design
1083   of activate off the U.S. East Coast, Bull. Am. Meteorol. Soc., 100(8), 1511–1528,
1084   https://doi.org/10.1175/BAMS-D-18-0100.1, 2019.
1085 Sorooshian, A., Corral, A. F., Braun, R. A., Cairns, B., Crosbie, E., Ferrare, R., Hair, J., Kleb, M.
1086   M., Hossein Mardi, A., Maring, H., McComiskey, A., Moore, R., Painemal, D., Scarino,
1087   A. J., Schlosser, J., Shingler, T., Shook, M., Wang, H., Zeng, X., Ziemba, L. and Zuidema,
1088   P.: Atmospheric Research Over the Western North Atlantic Ocean Region and North
1089   American East Coast: A Review of Past Work and Challenges Ahead, J. Geophys. Res.
1090   Atmos., in press, https://doi.org/10.1029/2019JD031626, 2020.
1091 Strapp, J. W., Leaitch, W. R. and Liu, P. S. K.: Hydrated and dried aerosol-size-distribution
1092   measurements from the Particle Measuring Systems FSSP-300 probe and the deiced

PCASP-100X probe, J. Atmos. Ocean. Technol., 9(5), 548–555, https://doi.org/10.1175/1520-0426(1992)009<0548:HADASD>2.0.CO;2, 1992.

Twomey, S.: The nuclei of natural cloud formation part II: The supersaturation in natural clouds and the variation of cloud droplet concentration, Geofis. Pura e Appl., 43(1), 243–249, https://doi.org/10.1007/BF01993560, 1959.

Twomey, S.: The influence of pollution on the shortwave albedo of clouds, J. Atmos. Sci., 34, 1149–1152, https://doi.org/10.1175/1520-0469(1977)034<1149:TIOPOT>2.0.CO;2, 1977.

Van Dingenen, R., Raes, F. and Jensen, N. R.: Evidence for anthropogenic impact on number concentration and sulfate content of cloud-processed aerosol particles over the North Atlantic, J. Geophys. Res. Atmos., 100(D10), 21057–21067, https://doi.org/10.1029/95jd02141, 1995.

Wang, Z., Sorooshian, A., Prabhakar, G., Coggon, M. M. and Jonsson, H. H.: Impact of emissions from shipping, land, and the ocean on stratocumulus cloud water elemental composition during the 2011 E-PEACE field campaign, Atmos. Environ., 89, 570–580, https://doi.org/10.1016/j.atmosenv.2014.01.020, 2014.

Wang, Z., Mora Ramirez, M., Dadashazar, H., MacDonald, A. B., Crosbie, E., Bates, K. H., Coggon, M. M., Craven, J. S., Lynch, P., Campbell, J. R., Azadi Aghdam, M., Woods, R. K., Jonsson, H., Flagan, R. C., Seinfeld, J. H. and Sorooshian, A.: Contrasting cloud composition between coupled and decoupled marine boundary layer clouds, J. Geophys. Res. Atmos., 121(19), 11679–11691, https://doi.org/10.1002/2016JD025695, 2016.

West, R. E. L., Stier, P., Jones, A., Johnson, C. E., Mann, G. W., Bellouin, N., Partridge, D. G. and Kipling, Z.: The importance of vertical velocity variability for estimates of the indirect aerosol effects, Atmos. Chem. Phys., 14(12), 6369–6393, https://doi.org/10.5194/acp-14-6369-2014, 2014.

Wonaschütz, A., Coggon, M., Sorooshian, A., Modini, R., Frossard, A. A., Ahlm, L., Mülmenstädt, J., Roberts, G. C., Russell, L. M., Dey, S., Brechtel, F. J. and Seinfeld, J. H.: Hygroscopic properties of smoke-generated organic aerosol particles emitted in the marine atmosphere, Atmos. Chem. Phys., 13(19), 9819–9835, https://doi.org/10.5194/acp-13-9819-2013, 2013.

Xue, H. and Feingold, G.: A modeling study of the effect of nitric acid on cloud properties, J. Geophys. Res., 109, D18204, https://doi.org/10.1029/2004JD004750, 2004.

1125   **Table 1.** Summary of field campaign data sets used in this study and statistics related to cloud
1126   water sample collection. Smoke-influenced RFs were NiCE RFs 16–23 and FASE RFs 3–11 and
1127   13–15.
1128

Field campaign	Dates (mm/dd/yyyy)	# of RFs	# of samples	# of fire-impacted samples
Eastern Pacific Emitted Aerosol Cloud Experiment (E-PEACE)	07/08/2011 – 08/18/2011	30	82	0
Nucleation in California Experiment (NiCE)	07/08/2013 – 08/07/2013	23	119	31
Biological and Oceanic Atmospheric Study (BOAS)	07/02/2015 – 07/24/2015	15	29	0
Fog and Stratocumulus Evolution Experiment (FASE)	07/18/2016 – 08/12/2016	16	155	136

1129

1130 **Table 2.** Summary of chemical species analyzed in this study. IC = ion chromatography; ICP =
1131 ICP-MS or ICP-QQQ. Note: NSS species, with the exception of NSS-SO$_4^{2-}$, were calculated
1132 using elements, not ions, hence they have no superscript charge.
1133

Elements (ICP)				Inorganic ions (IC)		Organic ions (IC)	
1	Ag	24	Na	47	Ammonium (NH$_4^+$)	66	Acetate
2	Al	25	Nb	48	Bromide (Br$^-$)	67	Adipate
3	As	26	Ni	49	Calcium (Ca^{2+})	68	Butyrate
4	B	27	P	50	Chloride (Cl$^-$)	69	Formate
5	Ba	28	Pb	51	Fluoride (F$^-$)	70	Glutarate
6	Br	29	Pd	52	Lithium (Li$^+$)	71	Glycolate
7	C	30	Rb	53	Magnesium (Mg^{2+})	72	Glyoxylate
8	Ca	31	Rh	54	Methanesulfonic acid (MSA)	73	Lactate
9	Cd	32	Ru	55	Nitrate (NO$_3^-$)	74	Maleate
10	Cl	33	S	56	Nitrite (NO$_2^-$)	75	Malonate
11	Co	34	Sb	57	Potassium (K$^+$)	76	Oxalate
12	Cr	35	Se	58	Sodium (Na$^+$)	77	Propionate
13	Cs	36	Si	59	Sulfate (SO$_4^{2-}$)	78	Pyruvate
14	Cu	37	Sn			79	Succinate
15	Fe	38	Sr		**Amines (IC)**		
16	Ga	39	Ta	60	Diethylamine (DEA)		**Acidity (pH)**
17	Hf	40	Te	61	Dimethylamine (DMA)	80	Hydrogen ion (H$^+$)
18	I	41	Ti				
19	K	42	V		**NSS species (calculated)**		
20	Li	43	W	62	NSS Calcium (NSS-Ca)		
21	Mg	44	Y	63	NSS Potassium (NSS-K)		
22	Mn	45	Zn	64	NSS Magnesium (NSS-Mg)		
23	Mo	46	Zr	65	NSS Sulfate (NSS-SO$_4^{2-}$)		

1134

1135 **Table 3.** Summary of one-predictor models for N_d based on using any of nine of the final
1136 chemical species that were identified after applying the filtering scheme shown in Figure 2. The
1137 coefficients correspond to a linear model of the form $\log(N_d) = a_0 + a_1 \log(M_i)$, where M_i is the
1138 mass concentration of species i.
1139

Species	R^2_{adj}	Coefficients	
		a_0	a_1
Tot-SO$_4^{2-}$	0.40	2.05	0.32
NH$_4^+$	0.34	2.33	0.25
NSS-SO$_4^{2-}$	0.29	2.13	0.28
MSA	0.26	2.37	0.31
NO$_3^-$	0.24	2.12	0.25
Na	0.19	2.03	0.13
Ox	0.15	2.26	0.18
V	0.14	2.61	0.15
Fe	0.05	2.26	0.09

1140

1141 **Table 4.** Comparison of coefficient values for studies that correlate N_d to SO_4^{2-} (total or non-sea
1142 salt). The coefficients correspond to a linear model of the form $\log(N_d) = a_0 + a_1 \log(SO_4^{2-})$.
1143

Reference	a_0	a_1	SO_4^{2-}	R^2	Cloud type
Leaitch et al. (1992)[a]	1.95	0.257	Tot	0.3	Continental stratocumulus
	2.33	0.186	Tot	0.49	Continental cumulus
Novakov et al. (1994)	2.323	0.091	NSS	0.50[b]	Marine stratocumulus
	2.43	-0.056	NSS	0.03	Marine cumulus
Van Dingenen et al. (1995)[c]	2.33	0.4	NSS	0.42	All cloud types combined
Boucher & Lohmann (1995)[c]	2.24	0.257	NSS	[d]	Continental stratus
	2.54	0.186	NSS	[d]	Continental cumulus
	2.06	0.48	NSS	[d]	Marine
	2.21	0.41	NSS	[d]	All cloud types combined
Saxena & Menon (1999)	0.67	0.66	Tot	[d]	Continental orographic clouds
Lowenthal et al. (2004)	2.32	0.74	NSS	0.82	Marine
	2.38	0.49	NSS	0.66	Continental
	2.39	0.5	NSS	0.81	Combined
McCoy et al. (2017)	2.11	0.41	NSS	0.36	Marine stratocumulus

[a] The units of SO_4^{2-} for this regression are nEq m^{-3}. All other studies report SO_4^{2-} in units of μg m^{-3}.
However, the value of the slope (a_1) is not affected by the units of concentration.

[b] The R^2 has a $p > 0.05$ due to having few data points.

[c] These regressions were made using data compiled from several studies and assume that $N_{CCN} \sim N_d$.

[d] Study does not report R^2.

1144

Table 5. The top three statistically significant regressions with the highest R^2_{adj} for a given number of predictors. The coefficients correspond to a linear model of the form $\log(N_d) = a_0 + \Sigma\ a_i \log(P_i)$.

# of Predictors	Predictors (P_i) and their respective coefficients (a_i)											R^2_{adj}
	a_0	a_1	P_1	a_2	P_2	a_3	P_3	a_4	P_4	a_5	P_5	
1	2.05	0.32	Tot-SO$_4^{2-}$									0.40
	2.33	0.25	NH$_4^+$									0.34
	2.13	0.28	NSS-SO$_4^{2-}$									0.29
2	2.18	0.22	Tot-SO$_4^{2-}$	0.12	NH$_4^+$							0.48
	2.43	0.21	MSA	0.15	NH$_4^+$							0.44
	2.25	0.19	NH$_4^+$	0.09	Na							0.42
3	2.25	0.13	NSS-SO$_4^{2-}$	0.13	NH$_4^+$	0.10	Na					0.50
	2.24	0.19	Tot-SO$_4^{2-}$	0.10	Ox	0.07	NH$_4^+$					0.49
	2.25	0.17	Tot-SO$_4^{2-}$	0.11	NH$_4^+$	0.08	MSA					0.49
4	2.32	0.21	Tot-SO$_4^{2-}$	0.20	Ox	0.09	NH$_4^+$	-0.15	NO$_3^-$			0.52
	2.29	0.11	NSS-SO$_4^{2-}$	0.10	Ox	0.09	Na	0.08	NH$_4^+$			0.51
	2.31	0.11	NH$_4^+$	0.10	NSS	0.10	MSA	0.08	Na			0.51
5	2.10	0.13	Na	0.12	Ox	0.11	NSS-SO$_4^{2-}$	0.08	NH$_4^+$	-0.05	V	0.56
	2.40	0.23	Ox	0.13	NSS-SO$_4^{2-}$	0.10	NH$_4^+$	0.09	Na	-0.17	NO$_3^-$	0.55
	2.36	0.14	NH$_4^+$	0.14	MSA	0.12	NSS-SO$_4^{2-}$	0.07	Na	-0.08	NO$_3^-$	0.52

1150 **Table 6.** Comparison of regressions containing NSS-SO$_4^{2-}$, Na, and Ox.

1151

# of Predictors	Predictors (P_i) and their respective coefficients (a_i)							
	a_0	a_1	P_1	a_2	P_2	a_3	P_3	R^2_{adj}
1	2.13	0.28	NSS-SO$_4^{2-}$					0.29
2	2.12	0.23	NSS-SO$_4^{2-}$	0.12	Na			0.40
	2.26	0.24	NSS-SO$_4^{2-}$	0.12	Ox			0.34
3	2.22	0.22	NSS-SO$_4^{2-}$	0.10	Na	0.08	Ox	0.42

1152

Table 7. Results of multivariable regressions from previous studies that have correlated N_d to mass concentrations. The regression corresponds to a model like Equation 3. OM = Organic Matter, SS = Sea Salt, BC = Black Carbon, DU = Dust.

Reference	a_0	a_1	P_1	a_2	P_2	a_3	P_3	a_4	P_4	R^2	Cloud type
Menon et al. (2002)[a]	2.41	0.50	NSS-SO$_4^{2-}$	0.13	OM						Continental
	2.41	0.50	NSS-SO$_4^{2-}$	0.13	OM	0.05	SS				Marine
McCoy et al. (2017)	1.78	0.31	NSS-SO$_4^{2-}$	-0.19	SS	0.057	BC	0.031	DU	0.44	Marine stratocumulus (global average)
McCoy et al. (2018)	2.03	0.2	NSS-SO$_4^{2-}$	-0.04	SS	-0.03	BC	0	DU	0.08	Marine stratocumulus (just Californian coast)

[a] This study obtains data from other studies and calculates organic matter.

1158   **Table 8.** Summary of the R^2_{adj} obtained when correlating mass concentration of a species to N_d
1159   under different atmospheric conditions.
1160

Binning criterion	Data points considered	R^2_{adj}			
		NSS-SO$_4^{2-}$	Na	Ox	Fe
None	All	0.29	0.19	0.15	0.05
Turbulence	High σ_w	0.27	0.26	0.09	0.02[a]
	Low σ_w	0.27	0.09	0.30	0.07
Smoke influence	No smoke	0.36	0.24	0.07	0.04
	Smoke	0.22	0.17	0.42	0.15
	NiCE[b]	0.36	0.46	0.60	0.28
	FASE[b]	0.18	0.13	0.41	0.12
Normalized cloud height	Top third	0.33	0.33	0.08	0.03
	Middle third	0.29	0.16	0.16	0.03
	Bottom third	0.17	0.10	0.29	0.20

[a] This R^2_{adj} has a p-value > 0.05.

[b] Only smoke-influenced samples in this campaign were considered.

1161
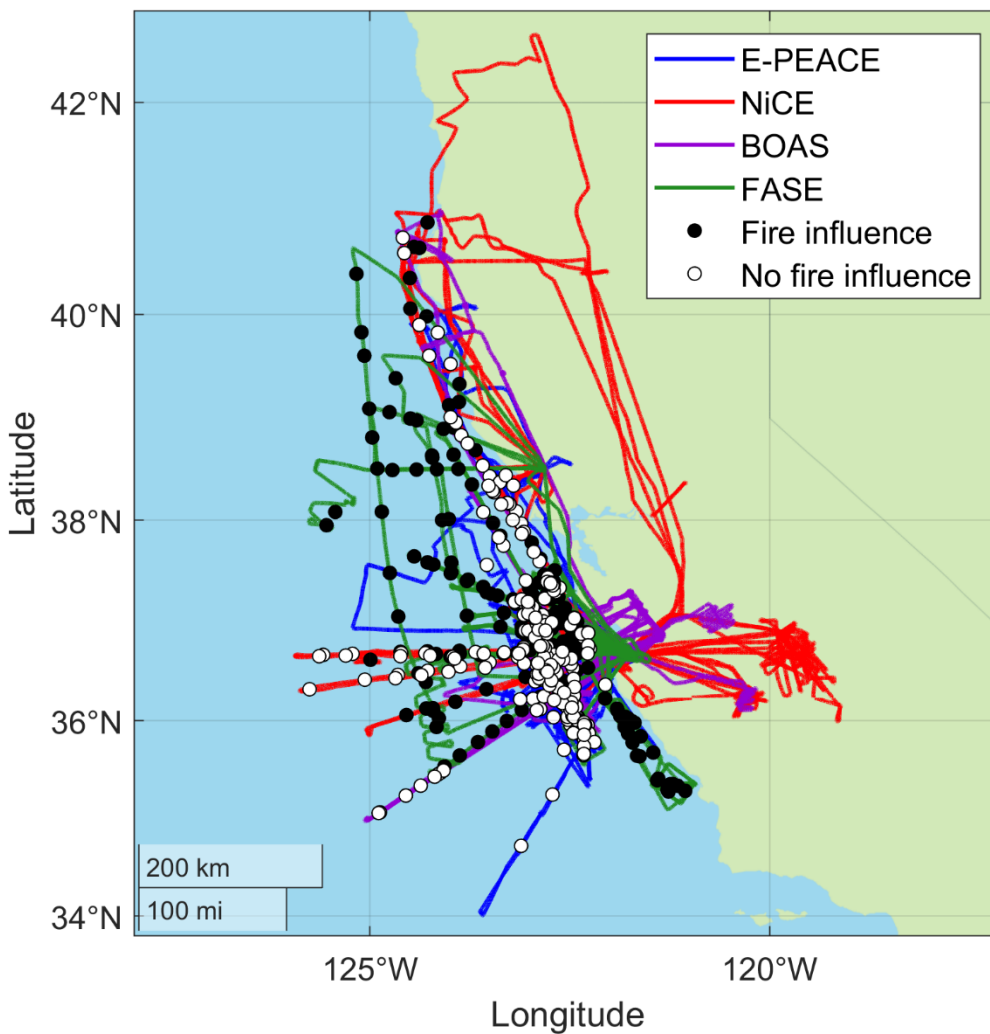
1162
1163 **Figure 1.** Flight paths for each of the four campaigns used in this study. Markers indicate the
1164 average location at which the cloud water samples were collected. Smoke- and non-smoke-
1165 influenced samples are indicated with filled and open markers, respectively.
1166
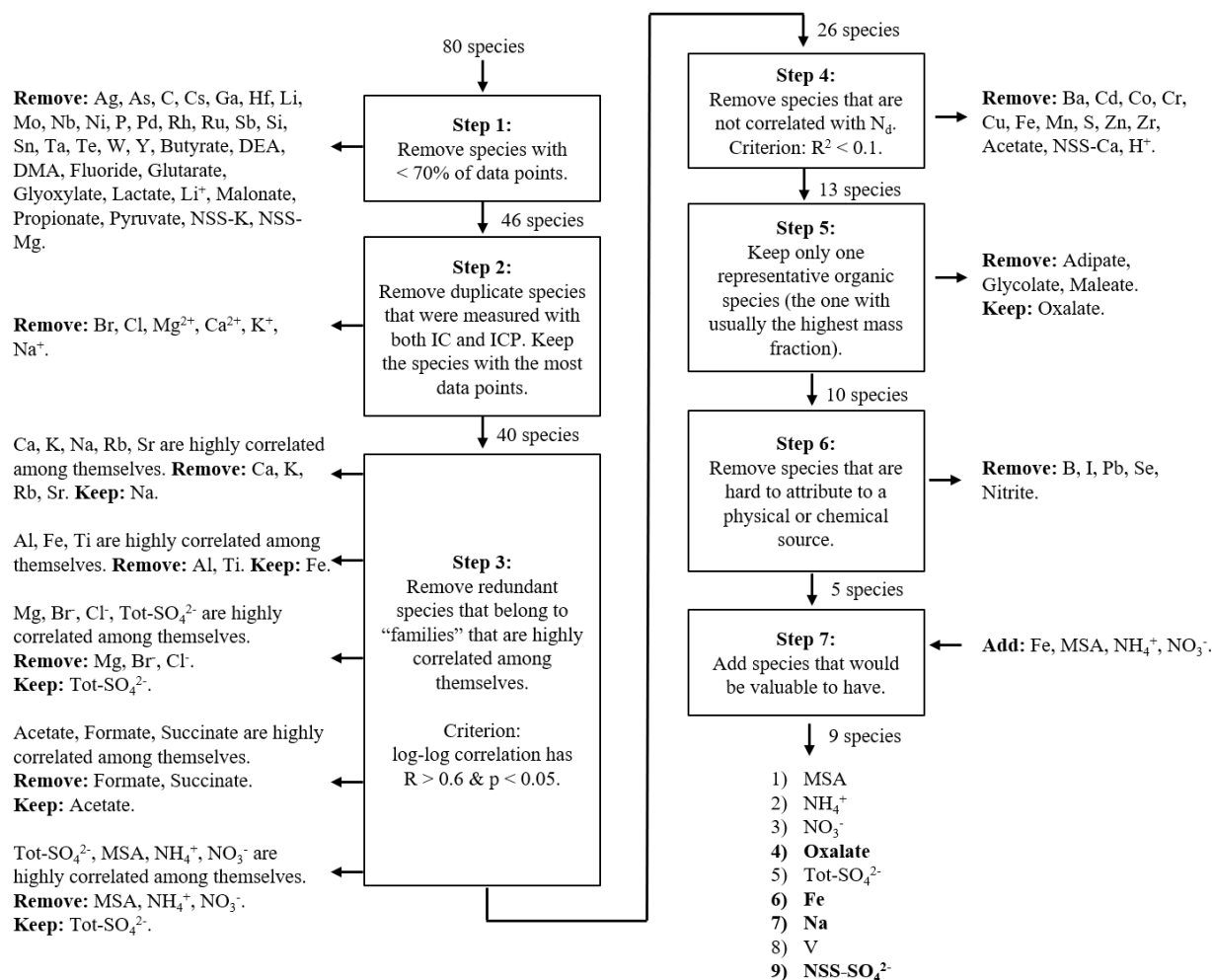
1167
1168 **Figure 2.** Algorithm used to filter the number of species from 80 to 9. The four bolded species
1169 are the ones used in Section 3.3). ICP = ICP-MS + ICP-QQQ.
1170
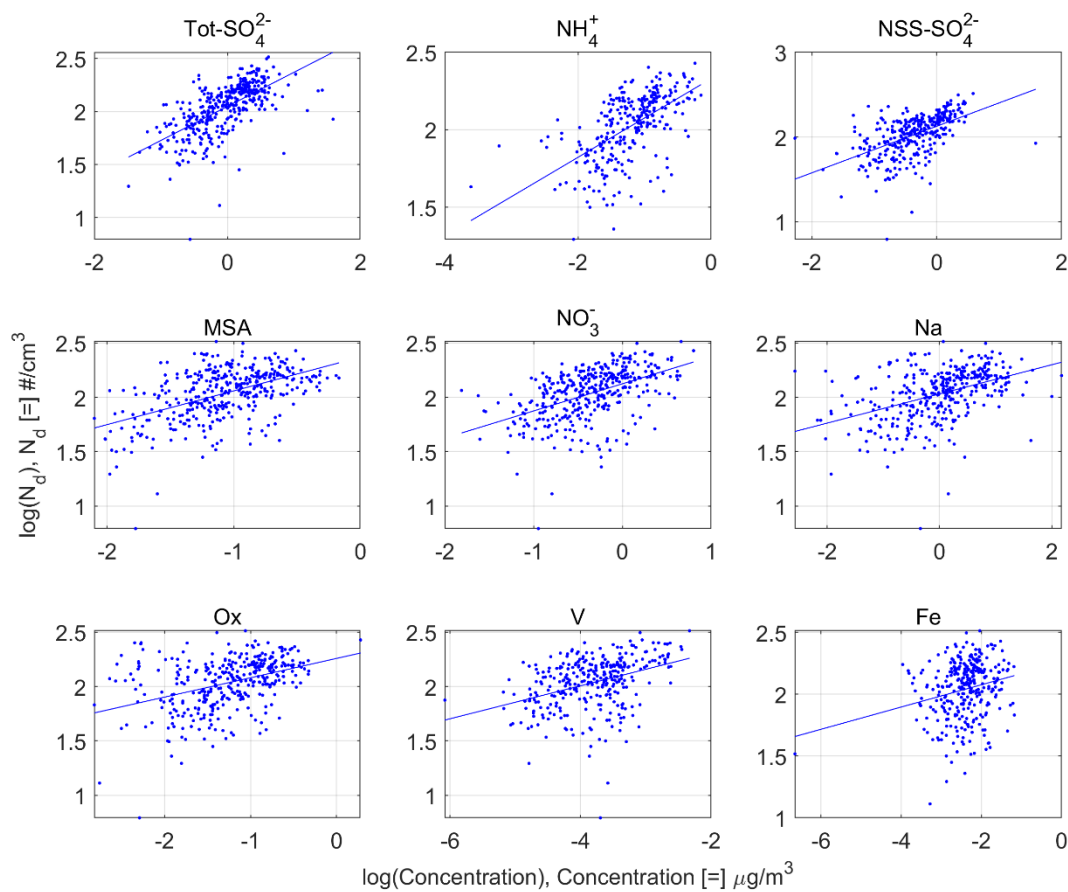
1171
Figure 3. Scatter plot for the nine filtered species from Figure 2. The lines are linear regression
models of the form $\log(N_d) = a_0 + a_1 \log(M_i)$, where M_i is the mass concentration of species i.
1174
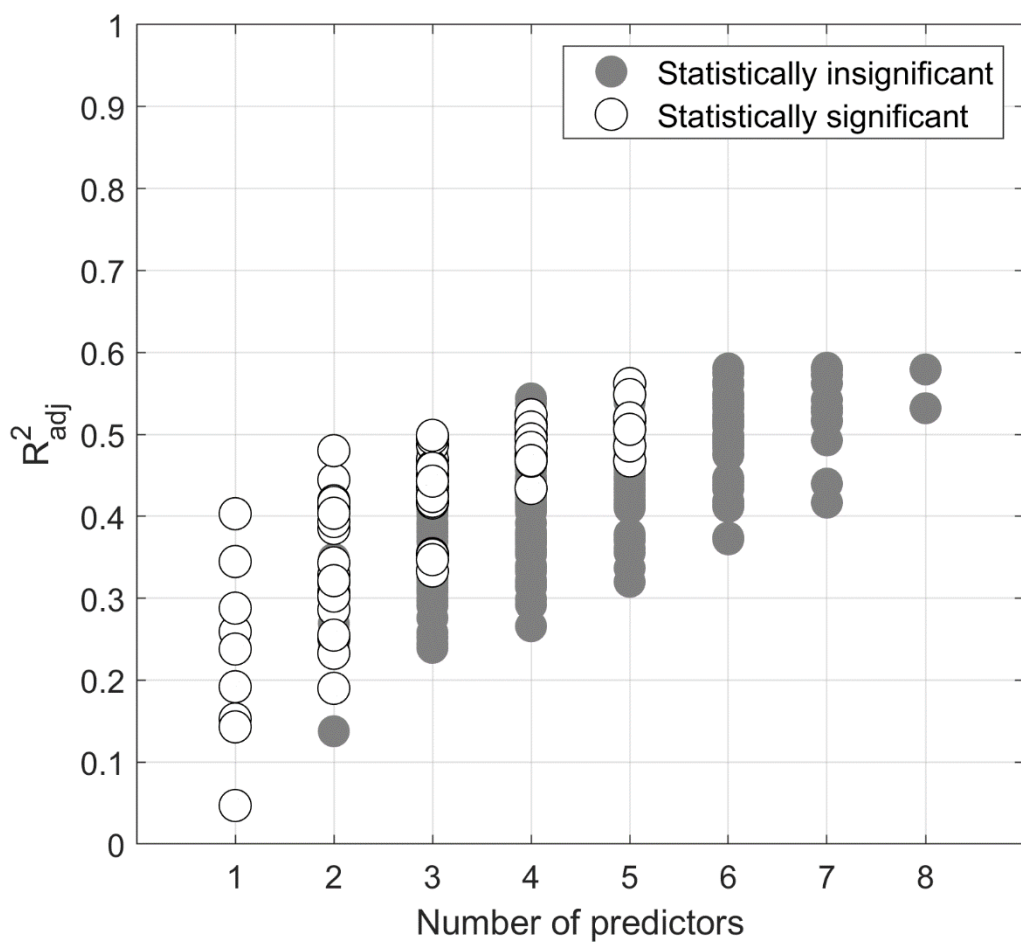
1175
1176 **Figure 4.** Plot showing which of the 383 regressions are statistically significant. This plot
1177 ignores the regressions that use both NSS-SO_4^{2-} and Tot-SO_4^{2-} simultaneously.
1178
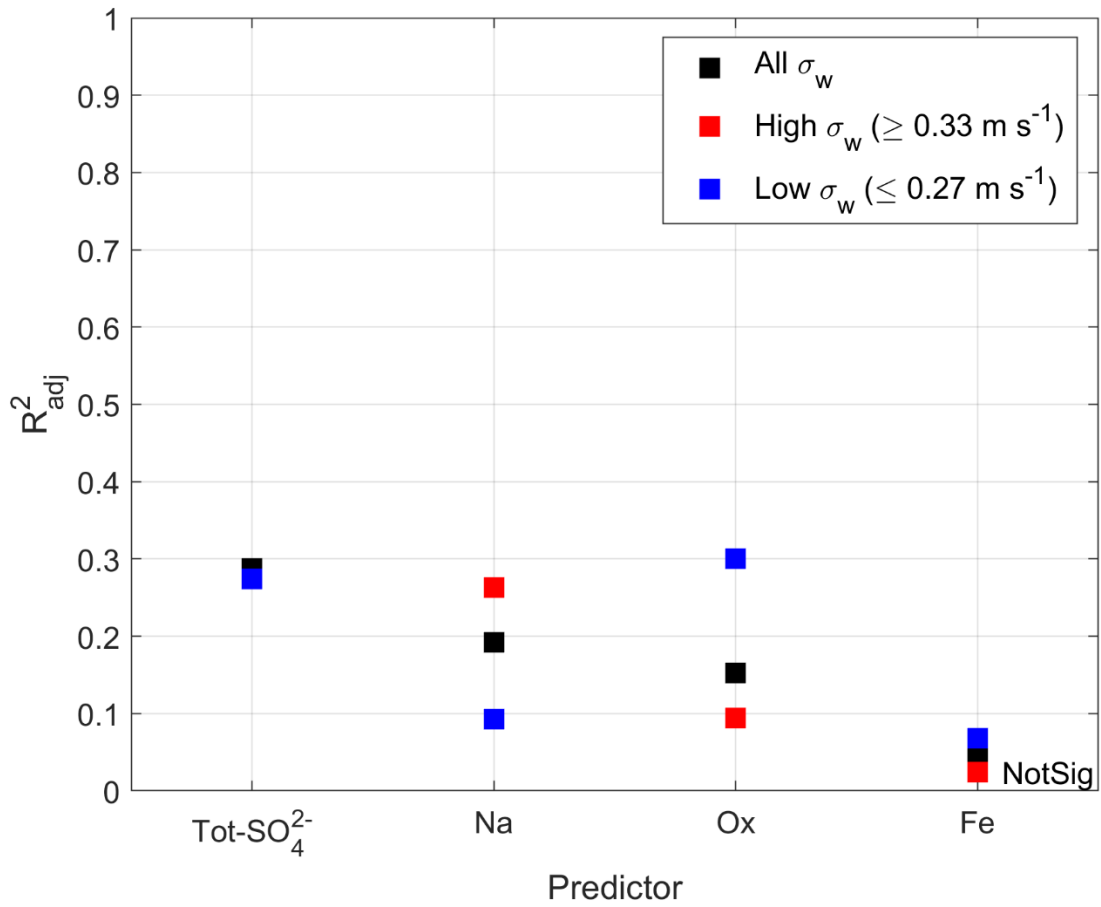
1179
1180 **Figure 5.** Effect of turbulence (quantified using σ_w) on the ability of a single species to predict
1181 N_d. For NSS-SO$_4^{2-}$, the high (red) and low (blue) σ_w data points overlap. NotSig = Not
1182 statistically significant according to the definition in Section 2.5.
1183
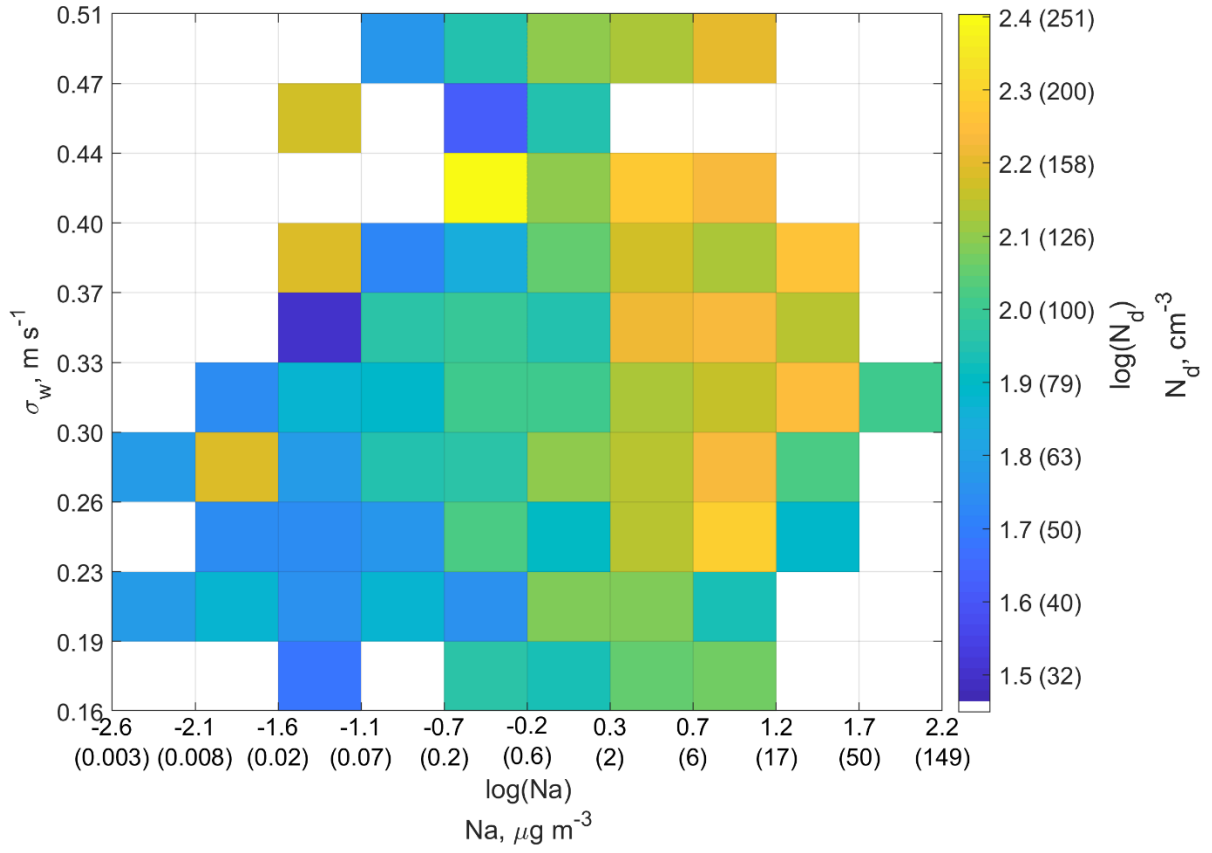
1184
1185 **Figure 6.** Heatmap showing the dependence of N_d on both σ_w and Na. The lower and upper
1186 bounds for the x-axis, y-axis, and color bar cover the entire range of σ_w, Na, and N_d, respectively.
1187 To assist in physical interpretation, the tick markings on the x-axis and color bar show two
1188 numbers: those without parenthesis correspond to log(Na) or log(N_d); those within parenthesis
1189 correspond to Na or N_d, in their respective units.
1190
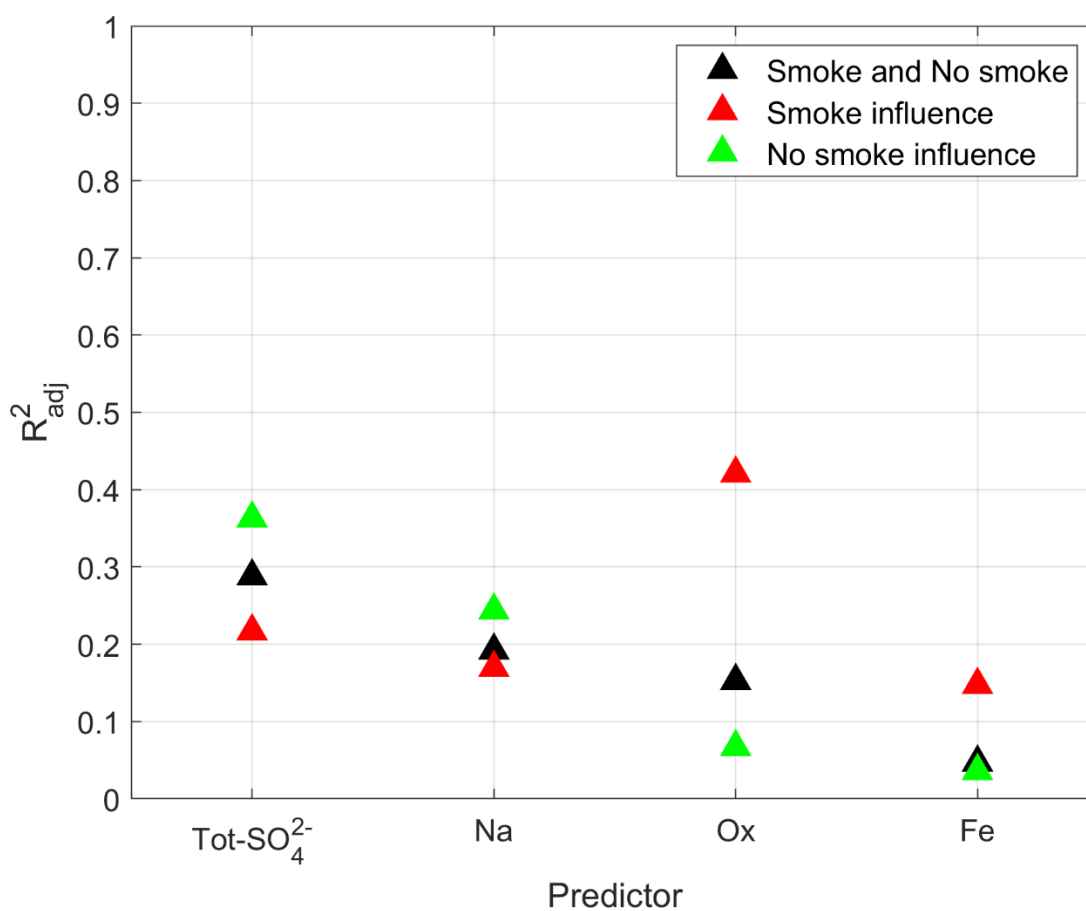
Figure 7. Effect of the influence of smoke on the ability of a single species to predict N_d.
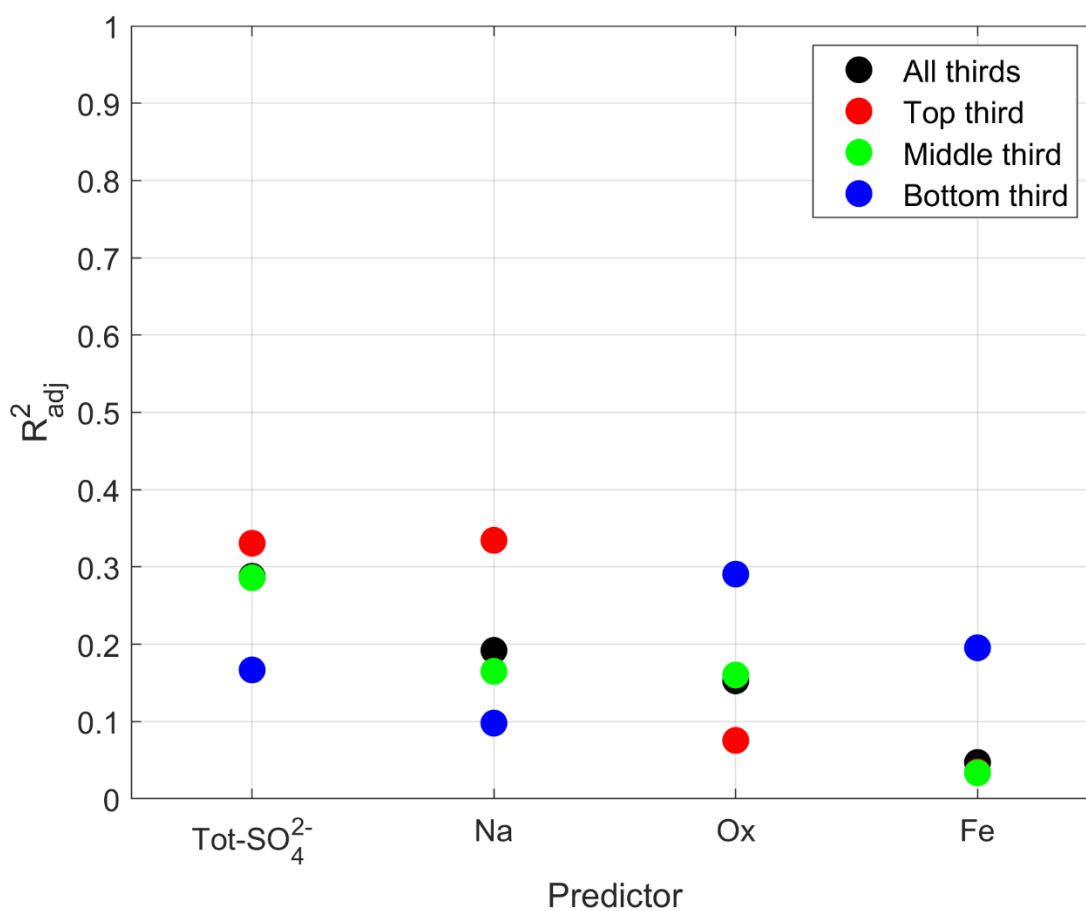
1194
1195 **Figure 8.** Effect of the influence of normalized cloud height on the ability of a single species to
1196 predict N_d. For Fe, the top 3rd (red) data point overlaps with the middle and bottom 3rd (green and
1197 blue) data points.
1198